DEVELOPMENT OF A NEW TEST SPECIMEN WITH TAPERED CROSS-SECTION FOR USE IN UNIAXIAL FATIGUE TESTING OF HOT MIX ASPHALT

A THESIS SUBMITTED TO THE GRADUATE DIVISION OF THE UNIVERSITY OF HAWAIʻI AT MĀNOA IN PARTIAL FULFILLMENT OF THE REQUIREMENTS FOR THE DEGREE OF
MASTER OF SCIENCE

IN

CIVIL ENGINEERING

MAY 2018

By

Grant John Karr

Thesis Committee:

Adrian R. Archilla, Chairperson
Ian Robertson
Tianwei Ma

Keywords: Hot Mix Asphalt, Asphalt Concrete Fatigue, Asphalt Concrete Performance Testing

ACKNOWLEDGEMENTS

I would first like to thank my thesis committee members, Dr. David Ma and Dr. Ian Robertson, for their significant assistance throughout the course of my thesis work and general guidance during my graduate studies. I would also like to thank Grace Pacific, LLC, in particular Mr. Jeromy Castro, for providing aggregate and hot mix asphalt samples. This generous donation of time and resources helped tremendously in carrying out the experiments.

Additionally, I would like to express my deepest gratitude to my faculty advisor and thesis committee chair, Dr. Adrian Archilla. None of my success would have been possible without your incredible guidance and enthusiasm in helping me grow academically. I truly appreciate all you have done, and I look forward to seeing you and your work continue to excel.

ABSTRACT

Despite recent developments, two primary challenges associated with fatigue testing of asphalt concrete cylinders remain: end failures and applicability to in-situ samples. End failures, or failure regions developing outside the strain gauge length, occur frequently and significantly reduce the value of the test. Samples cored from the field are often made up of several construction lifts ranging from 38 – 150 mm, rendering it incompatible with standard test cylinder dimensions. This study proposes a modified specimen geometry for use in fatigue testing of asphalt concrete mixtures which addresses these two challenges. The proposed configuration is a prismatic specimen which can be sliced horizontally from a cylinder with a diameter of 150 mm. The dimensions of the specimen are 110 mm long by 100 mm wide with variable thickness. The specimen width is tapered along the longitudinal axis to encourage middle failures. Constant crosshead fatigue tests are performed on test specimens as a proof of concept.

TABLE OF CONTENTS

LIST OF TABLES

LIST OF FIGURES

LIST OF ABBREVIATIONS AND SYMBOLS

AASHTO	American Association of State Highway and Transportation Officials
AC	Asphalt Content
AMPT	Asphalt Mixture Performance Tester
AV	Air Void (Content)
G_{mb}	Bulk Specific Gravity
G_{mm}	Maximum Specific Gravity
HMA	Hot Mix Asphalt
LVDT	Linear Variable Differential Transformer
NCHRP	National Cooperative Highway Research Program
NMAS	Nominal Maximum Aggregate Size
RAP	Recycled Asphalt Pavement
SBS	Styrene-Butadiene-Styrene
SGC	Superpave Gyratory Compactor
SHRP	Strategic Highway Research Program
SPT	Simple Performance Test(er)
SSD	Saturated Surface Dry

CHAPTER 1: INTRODUCTION

1.1 Introduction

Fatigue cracking of asphalt concrete is a fundamental consideration in the design of flexible pavements. The onset of fatigue cracking greatly affects the performance and safety of the pavement, and results in significant maintenance and rehabilitation costs. In order to effectively address the issue, there is a critical need for fatigue tests that can efficiently but reliably characterize the fatigue performance of asphalt concrete.

For the majority of the 20th century, fatigue tests were primarily flexural or indirect tension tests. The uniaxial fatigue test began gaining popularity near the beginning of the 21st century as a result of two significant developments: The Simple Performance Tester (SPT) and the application of continuum damage theory to the behavior of asphalt concrete. The SPT is now more commonly referred as the Asphalt Mixture Performance Tester or AMPT, which is the term that will be used herein in this thesis. The AMPT is a versatile testing machine which tests the performance of asphalt mixtures. Among other tests, the AMPT is capable of performing uniaxial tests on cylindrical asphalt concrete specimens in stress or strain-controlled modes. The development of the AMPT, occurred around the same time researchers were applying the theory of continuum damage to asphalt concrete. This approach allows for the characterization and prediction of fatigue performance of asphalt mixtures based on uniaxial loading conditions. The combination of these two developments has led to an increased interest in uniaxial fatigue testing of asphalt concrete.

In general, uniaxial fatigue tests consist of applying cyclic loading to a cylindrical test specimen in a controlled-stress, controlled-strain, or controlled-crosshead mode. As the specimen is

continually loaded, fatigue damage is incurred by a gradual reduction in the specimen's ability to resist deformation. The tests continue until a pre-defined failure criterion is achieved. The behavior of the specimen is monitored by linear variable differential transformer (LVDT) strain gauges attached to the middle of the specimen. The test is relatively straight forward and intentionally compatible with AMPT systems, however there are challenges associated with the current specimen configuration. This study focuses on two challenges in particular: tests resulting in end failures and applicability of the test to samples obtained from the field.

Although complete fracture is not always necessary, the majority of failure criteria involve conditions with formation of macro-cracks. If these macro-cracks form outside the gauge length of the specimen, the LVDTs are unable to capture the behavior of the specimen in the region of failure and the value of the test is significantly limited. Formation of failure regions outside the gauge length of the LVDTs is referred to as an end failure and they are a common occurrence for this typical fatigue test method. There are multiple causes of end failures. The air void content of gyratory compacted cylinders is known to be higher near their ends (top and bottom) whereas fatigue strength is inversely related to air void content. Thus, failure in fatigue has a higher probability of occurring near the ends of the test specimen. In addition to the uneven air void content distribution, the test specimen must be gripped at the ends in order to apply a tensile load. This grip is typically achieved via a bonding agent. The steel loading platens, to which the specimen is bonded, have significantly higher stiffness than the asphalt concrete. This difference in stiffness results in a significant amount of strain concentration at the ends due to lateral restraint imposed through the bonded interface. Furthermore, even if the air void content were perfectly homogenous throughout the depth of the specimen and the loading could be applied

with an ideal gripping system producing no lateral restraint at the ends, the probability of the failure occurring between the gauge points would still be approximately equal to the ratio of the gauge length to the overall cylinder length.

The AMPT (SPT) was originally developed for mechanical testing of mixes prepared with a Superpave Gyratory Compactor (SGC). Superpave refers to a mix design method developed by the Strategic Highway Research Program in which the SGC is used to compact the asphalt concrete. The SGC was developed to simulate more closely the compaction process experienced by pavements constructed in the field. The Superpave design method involves compacting 150-mm diameter by 115-mm height hot-mix asphalt (HMA) cylinders in a gyratory compactor. These cylinders are tested for volumetric properties in order to understand expected results during construction of that mix.

For mechanical testing with the AMPT, 100-mm diameter by 150-mm height samples are cored and trimmed from larger compacted cylinders (150-mm diameter by 170-mm height). While the procedure is efficient for the laboratory produced specimens, this configuration does not conform to in-situ pavement samples cored from the field. Pavements are typically constructed in lifts which range in thickness from 38-mm to 150-mm. Therefore, 150-mm long cylinders cored from the field may contain multiple lifts with different mechanical properties.

The specimen geometry proposed in this study overcomes these two challenges without losing compatibility with standard AMPT procedures. The proposed specimen is prismatic, 110-mm long, 100-mm wide and the thickness can vary as needed with an ideal thickness of 38-mm. The narrow faces along the 110-mm long sides are continuously tapered by performing a 175 mm radius circumferential cut over the middle 90-mm the sample (i.e., starting 10 mm from the top

and bottom) and resulting in an 88-mm width at mid-depth. The tapered cross-section results in maximum strains developing at mid-depth, encouraging failure to occur in the middle, rather than at the ends even in the presence of some uneven air voids distribution. The proposed dimensions also allow for the specimen to be produced from a 150-mm diameter cylinder which makes it compatible with both gyratory compacted laboratory specimens and sample cylinders cored in the field. The thickness of the specimen can be as little as 25-mm, allowing for testing of field samples constructed in thin lifts. Finally, prior to testing, phenolic linen blocks are glued (using plastic steel putty) to steel loading platens and the specimen is subsequently glued to these blocks. The purpose of the blocks is two-fold: 1) the phenolic linen has a stiffness modulus between that of steel and asphalt concrete, reducing the effect of lateral restraint, and 2) the blocks make up for the difference in height between the 110-mm specimen and the standard 150-mm cylinder length required for use in the AMPT.

Overall, the substantial testing presented in this study shows that the proposed test specimens performed well in laboratory experiments. A process was developed to produce the specimen from standard gyratory compacted cylinders and subsequently test them in an AMPT. Once measures were put into place to reduce eccentric loading as much as possible, more than 95% of the correctly performed tests resulted in failure between the gauge points. The tests produce reasonable results and show a strong potential for use as a standard test to characterize the fatigue performance of asphalt mixtures. Further testing will reveal how well these specimens perform compared to their cylindrical counterparts and whether these specimens can be used for other performance tests.

CHAPTER 2: OBJECTIVES

2.1 Background

Fatigue cracking is one of the most important considerations in pavement design. Its characterization for asphalt mixtures has been of interest to pavement engineers for as long as asphalt has been used as a pavement material. Over the past several decades, researchers have developed test methods and analytical approaches to understand the fatigue strength characteristics of different asphalt mixtures subject to different load, temperature and frequency combinations. A summary of these developments is included in *CHAPTER 3: SUMMARY OF FATIGUE TEST METHODS*.

The first few decades of fatigue testing of asphalt concrete consisted primarily of flexure and indirect tensile tests. Over the last two decades, however, the uniaxial direct tension fatigue test has become a popular method for evaluating fatigue strength. The popularity of this test increased with the development of a continuum damage model (Park, Kim, & Schapery, 1996) which uncouples the effects of viscoelasticity and damage for asphalt loaded beyond its linear viscoelastic range through the use of an elastic-viscoelastic correspondence principle developed by Schapery (Schapery, 1984). Since this development, a significant amount of research focused on the use of continuum damage mechanics to model and analyze uniaxial fatigue testing of asphalt mixtures. This shift in focus enabled the uniaxial test procedure to become one of the primary methods of performing fatigue tests.

As the theory for the uniaxial fatigue behavior of asphalt developed, the uniaxial fatigue test procedure itself evolved as well. The National Cooperative Highway Research Program's (NCHRP) Project 9-29 developed a concept called the Simple Performance Tester (SPT). The

overall intent of the SPT is to provide a means of systematically and efficiently testing the performance of mixtures designed using the Superpave mix design method. The Superpave mix design method includes producing sample cylinders via a gyratory compactor which is intended to replicate the compaction process exhibited in the field. The result of this project was the development of the Asphalt Mixture Performance Tester (AMPT). Using 100-mm diameter by 150-mm tall cylindrical test specimens cored from larger cylinders compacted with SGC, the AMPT can perform a variety of tests to assess the performance characteristics of the asphalt mixture (Bonaquist, 2008). One such test that is compatible with the AMPT is the American Association of State Highway and Transportation Officials (AASHTO) Provisional Standard TP-107: Determining the Damage Characteristic Curve of Asphalt Concrete from Direct Tension Cyclic Fatigue Tests. This test uses cyclic, uniaxial, direct-tension loading to determine damage characteristics of a specimen based on continuum damage theory. The detailed procedure is available in the AASHTO Provisional Standard (AASHTO, 2016). A summary of the procedure is provided below:

1. Prepare and compact asphalt samples per AASHTO T312
2. Age specimens in accordance with AASHTO R30
3. Core a 100-mm diameter test specimen from the center of the gyratory specimen
4. Cut an equal length from the top and bottom of the specimen to obtain a 150-mm long test specimen
5. Attach mounting studs at 120° for LVDT sensors (70-mm gauge length)
6. Using a gluing jig to ensure parallel faces, glue the loading platens to each end of the test specimen.

7. Connect the specimen to the load cell by bolting the loading platens directly to the load cell supports.
8. Perform uniaxial, cyclic loading with a constant actuator displacement amplitude until prescribed failure criteria is achieved.

This procedure forms the basis for performing other tests involving uniaxial tensile loading of asphalt cylinders.

2.2 Motivation for Study

While the uniaxial fatigue test has evolved into a commonly used test compatible with the AMPT system, several challenges remain. This study focuses on two issues in particular: end failure i.e., specimen fracture occurring outside the gauge length of the linear variable differential transformer (LVDT) sensors and applicability to thin lift field samples. These challenges are discussed in detail in the following sections.

2.2.1 End Failure

As fatigue testing of asphalt mixtures has evolved, many different definitions of failure have been proposed. However, regardless of the selected failure definition, all asphalt fatigue tests analyze the behavior of the test specimen as damage accumulates and, ultimately, fails. This failure typically takes the form of microcracks which coalesce into the formation and propagation of a macrocrack. The behavior of the specimen during this process is observed through the deformation of the specimen within the gauge length of the LVDT sensors and the corresponding loads applied by the machine loading ram. Consequently, the formation of the macrocrack must occur within the gauge length for the fatigue behavior to be accurately analyzed. If the cracking occurs outside this gauge length, the value of the test results is

significantly limited. Unfortunately, this occurs quite frequently in uniaxial fatigue tests even today. An example of an end failure is illustrated in Figure 1.

Figure 1: Example of an End Failure (A. Archilla & Corrales-Azofeifa, 2017)

2.2.1.1 Air Void Distribution

The occurrence of end failures is common in cyclic fatigue testing of cylindrical specimens. One prime example of this is a study by Hou et al. at North Carolina State University. The study involved performing strain-controlled, uniaxial cyclic fatigue testing of cylindrical samples in order to predict fatigue performance of mixtures using the continuum damage model. Of the 50 tests performed, 19 resulted in end failures (Hou, 2009). A recent study published in the ASTM Journal of Testing and Evaluation (Lee, Norouzi, & Kim, 2016) found that end failures occurred 68% of the time when using samples with 100-mm diameter and 150-mm length, i.e., the dimensions specified by AASHTO TP-107. This study determined that simply reducing the specimen length to 130-mm decreased the occurrence of end failures to 10%. This was attributed to the fact that air void content is significantly higher near the exterior of a gyratory compacted

specimen (Chehab, O'Quinn, & Kim, 2000). However, even if the test specimen's physical properties and stress-strain state were perfectly uniform over its entire length, the probability of the crack forming within the gauge length of the LVDTs would depend on the ratio of the gauge length (typically 70 mm) to the overall specimen length (typically 130-150 mm).

2.2.1.2 Strain Concentrations Due to Lateral Restraint

Fatigue cracking has historically been assumed to originate at the bottom of the asphalt layer due to high tensile strains induced by bending. However, there is growing evidence that fatigue cracking can initiate at the surface of the pavement well before fatigue cracks are expected to form at the bottom due to traditional bottom-up fatigue cracking. Archilla suggests higher temperatures may, at least partially, explain the top-down fatigue cracking phenomenon evident on Hawaiian and other high-temperature climate pavements. For a given pavement profile, the stiffness of the asphalt concrete is typically assumed to decrease with depth due to the higher frequencies experienced at the surface. However, high temperature can result in a temperature gradient that decreases significantly from the surface down. Since the stiffness of asphalt concrete decreases as the temperature increases, this temperature gradient may cause the stiffness profile to reverse. In other words, the stiffness of the pavement may increase with depth. This reduced relative stiffness results in the potential for tensile strains to develop due to deformations induced by the wheel load near the surface. (A. R. Archilla, 2015).

Uniaxial fatigue tests are typically performed at 20°C. However, pavements in Hawaii rarely experience temperatures this low, even less so during peak traffic demands. There is a need to understand fatigue behavior of asphalt at temperatures higher than the standard 20°C. The tests performed at the University of Hawaii therefore focus on tests at 40°C. These tests resulted in a

high number of end-failures, more than would be expected to result from non-uniform air void distributions alone. It was postulated that this tendency for end failures was due to the strain concentrations arising from the radial restraint enforced by the bonding agent at the interface between the specimen and the end plates. The concentrations are exaggerated at higher temperatures since an increase in temperature decreases the stiffness and increases the Poisson effect of asphalt mixtures

A study by Archilla used a simple linear elastic finite element analysis, using a static tensile load, to demonstrate the strain concentrations that arise. Using an elastic modulus and Poisson ratio consistent with that of a hot-mix asphalt at 40°C, the analysis showed strain magnitudes near the interface were approximately twice the nominal strain of the specimen (200 and 100 microstrain, respectively). These strain concentrations are believed to contribute to the tendency for the specimens to break near the ends (A. Archilla & Corrales-Azofeifa, 2017).

The existence of strain concentrations at the load transfer interface is not a novel concept. In fatigue testing of metals, the test specimens have a reduced cross-section in the region being analyzed (ASTM, 2016). In fact, performance tests on asphalt involving compression, such as the flow number test per AASHTO Standard Test Procedure TP-79 (AASHTO, 2016), acknowledge and address these end effects by using a membrane at the interface to minimize friction which would otherwise cause stress and strain concentrations.

2.2.2 Thin-Lift Samples

Another drawback of the standard uniaxial fatigue test is its lack of compatibility with field samples. Typical SPT procedures, including the uniaxial fatigue test, use specimens obtained from a Superpave gyratory compactor. The compacted specimens have a diameter of 150-mm

and heights up to 200-mm. The SPT specimens are cored from these compacted specimens, typically yielding cylinders with 150 mm height and 100 mm diameter. However, asphalt pavements constructed in the field are often much less than 150 mm, with overlay lifts sometimes as thin as 25 mm. Clearly, asphalt cylinders cored in the field will not be compatible with the standard SPT cylinder dimensions. This poses a significant problem in that laboratory studies cannot be compared against the performance of in-situ pavements.

2.3 Proposed Test Specimen Configuration

The objective of this study was to develop an asphalt test specimen configuration which could overcome the challenges discussed in the previous section: concentration of stresses and strains at the interface and applicability to samples cored from the field. The proposed specimen is a 100-mm wide, 110-mm long rectangular slice with a thickness of 25 or 38-mm. The longer sides are tapered by means of a 175-mm radius cut over a length of 90-mm resulting in a width of 88-mm at mid-height. Figure 2 demonstrates this configuration.

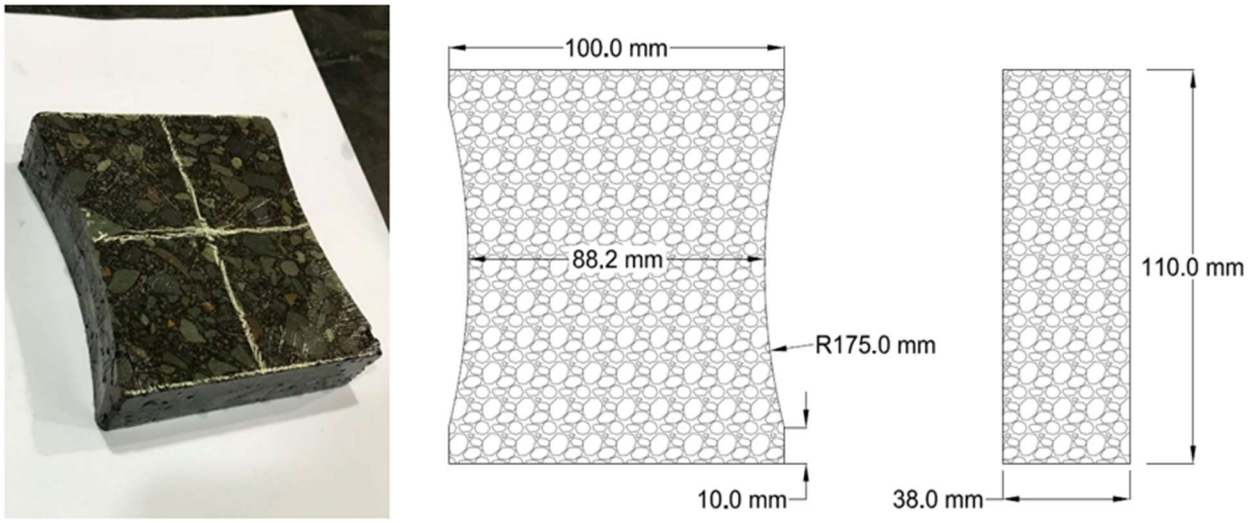

Figure 2: Proposed Specimen Configuration

The dimensions of this 'slice' orientation fall within the circumference of a 150-mm diameter cylinder. The thickness can be selected based on maximum nominal aggregate size of the mixture. The advantage of this configuration is its applicability to specimens produced in the lab per the typical 150-mm diameter gyratory compactor procedure, as well as 150-mm cored cylinders obtained from the field with various lift-thicknesses. In fact, depending on the height of the sample, one cylinder can produce multiple test specimens. Laboratory compacted specimens with a height greater than 110 mm will yield, at a minimum, 2 specimens.

The process of producing these test specimens is explained in detail in section *4.2 Specimen Preparation*. Figure 3 demonstrates the specimen preparation at various stages. A brief overview of the process is included below:

1. Produce 150-mm diameter asphalt mix specimen either compacted in the lab or cored from the field.
2. After obtaining volumetric properties of the full cylinder, slice approximately 15 to 20-mm from both ends of the cylinders and discard. (This step may not be applicable to field samples, as the full depth of the core may be required).
3. Cut as many slices as available from the remaining cylinder at desired thickness (38-mm typical).
4. Mark a 100 mm by 110 mm rectangle within the circumference of the discs and cut accordingly. It is important that each cut be made perpendicular to all adjacent surfaces. Adjust the platform and back support of the saw as needed to ensure perpendicularity to the blade. (more detail is provided in section 4.2 Specimen Preparation).

5. Using a trimming jig, cut an approximately 175-mm radius arc from the longitudinal (110-mm) sides with entry points 10-mm from each corner.
6. Ensure all cuts are square to adjacent edges and final dimensions are within a satisfactory margin.
7. Determine the bulk specific gravity of the specimen and calculate air void content.
8. Record all relevant geometric dimensions.
9. Age the specimen per AASHTO R30.
10. Glue gauge points to specimen as necessary to mount LVDTs on each face prior to testing.
11. Using sufficient bonding agent, glue phenolic linen interface blocks to steel plates. Center of interface blocks must align with center of steel plates.
12. After allowing bonding agent in previous step to reach initial set, glue the specimens to the linen interface blocks. It is imperative that the specimen be attached perpendicular to the interface blocks and steel plates. Use of adjustable aluminum braces are beneficial in ensuring a uniform bond thickness (see Figure 4).
13. Allow all bonded surfaces to reach full set.
14. Insert specimen into load cell and allow specimen and all testing equipment to condition to testing temperature.
15. Without removing braces, raise load cell into place and bolt steel plates to loading platens.
16. Maintain zero force until specimen reaches equilibrium then hold actuator displacement.

17. Modify loading parameters to achieve the desired constant crosshead displacement-controlled test.
18. Remove braces and run test.

Figure 3: Example of Proposed Specimen Production at Various Phases

Figure 4: Gluing Jig with Aluminum Braces

This test procedure is quite similar to the standard direct tension fatigue test for cylindrical specimens outlined in AASTHO TP-107 (AASHTO, 2016) . The first major difference is the additional cutting procedures required to produce the tapered specimens. The other major difference is the use of phenolic linen interface blocks between the steel plates and the asphalt specimen. These additional steps increase the test preparation time for a single specimen by approximately 30-60 minutes. However, a significant amount of time and material is saved because multiple specimens can be produced from a single compacted cylinder. As such, in addition to the added benefits of the specimen configuration mentioned earlier in this section, this proposed test specimen can be produced more efficiently than the standard cylindrical specimen configuration. A detailed description of the proposed process is provided in *4.2 Specimen Preparation.*

CHAPTER 3: SUMMARY OF FATIGUE TEST METHODS

3.1 Asphalt Mixture Fatigue Test Methods

Fatigue cracking has been one of the major forms of distress in asphalt pavement since its inception. The need for an understanding of fatigue behavior in asphalt was formally acknowledged in the middle of the 20th century (Hveem & Carmany, 1949). In the decades to follow, different fatigue test procedures were proposed and utilized by researchers. A brief summary of the different test methods is provided in the following sections. For a more detailed summary of these methods, two references in particular are recommended. A report by Porter and Kennedy at the University of Texas at Austin offers a thorough summary of the various test methods used in the 1960s and 1970s (Porter & Kennedy, 1975). A summary report by Tangella et al. as part of the Strategic Highway Research Program Project A-003-A provides an excellent overview of the wide variety of test methods proposed between 1950 and 1990 (Tangella, Craus, Deacon, & Monismith, 1990).

3.1.1 Flexural Fatigue Tests

The most popular fatigue test to emerge in the second half of the 20th century was the flexural fatigue test. The general concept of a flexural fatigue test is to induce a uniform bending moment over a portion of an asphalt concrete beam. Following conventional beam theory concepts, a given bending moment results in a known compressive or tensile strain at the extreme fibers of the beam. The bending moment is applied in a cyclic pattern until some pre-defined failure criterion is reached. The magnitude of the applied bending moment depends on whether the test is strain-controlled or stress-controlled. In a strain-controlled test, the magnitude of the bending moment is such that a given peak strain magnitude is achieved during each cycle. A stress-

controlled test repeatedly applies a bending moment such that the peak stress is equal for each cycle. Since the stiffness of asphalt concrete diminishes continuously throughout the duration of a fatigue test, the stress-controlled and strain-controlled tests behave in a significantly different manner.

One early test method that gained widespread popularity was that used by Deacon at the University of California at Berkeley (Deacon, 1965). Although not the first flexural test method, Deacon's flexural apparatus was the first to use a third-point bending system (now known as four-point bending) with simple supports. This form of load application yields a uniform bending moment along the middle segment of the test specimen. By monitoring the displacements along this segment, the fatigue behavior of the specimen can be associated to a known stress and strain distribution over a portion of the specimen, rather than a single point. A schematic of the third-point bending apparatus is shown in Figure 5. Third-point bending fatigue tests similar to that used by Deacon are still used today. This test method was utilized extensively by Monismith in the 1960s to investigate the fatigue behavior of various asphalt mixtures at the University of California at Berkeley. Results from these tests and similar flexural tests performed in other labs were summarized in a technical report for an ASTM symposium in 1971 (Epps & Monismith, 1972). An important conclusion drawn by Epps and Monismith from these fatigue tests is that "fatigue behavior of asphalt concrete mixtures are dependent upon a number of load, environmental, and mixture variables". In other words, the magnitude of the load or displacement applied during the fatigue test is insufficient in determining the fatigue behavior. Rest periods, temperature and air void content are examples of load, environmental and mixture variables, respectively, that can have a significant effect on the fatigue behavior.

The advantage of flexural fatigue tests is their direct correlation to the fatigue behavior of asphalt pavements in the field. The repeated bending of a compacted beam represents the continuous application of traffic loads on an asphalt pavement. As such, the performance of an asphalt mixture in a flexural fatigue test is a direct indicator of how that mixture will perform in the field as it pertains to fatigue cracking. Unfortunately, the equipment required to perform the test is large, expensive and specific to beam fatigue testing. Additionally, the test itself is cumbersome. Fatigue tests at low strain amplitudes can take as long as several days and the compaction process is atypical to the now standard gyratory compactor.

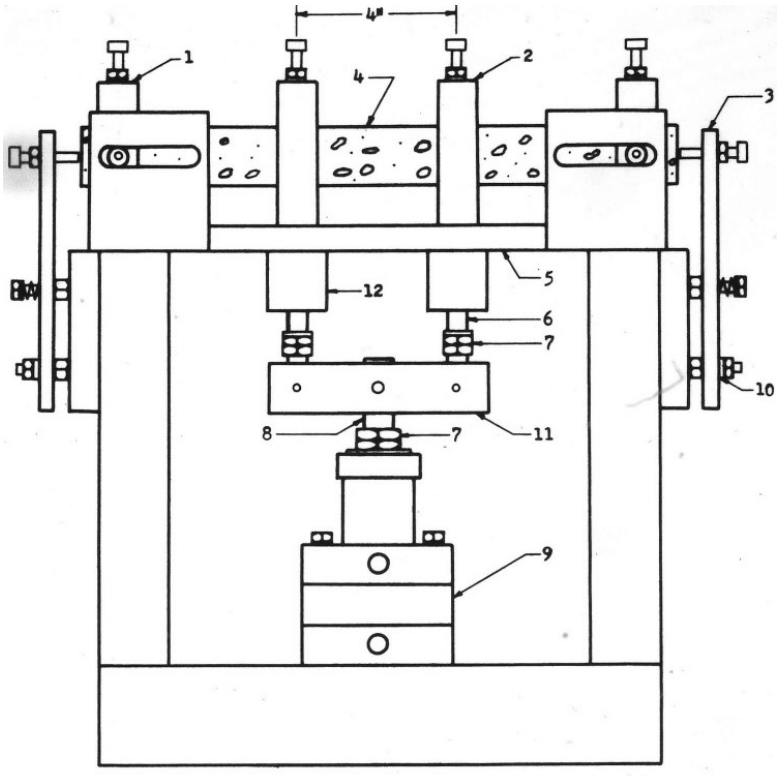

Figure 5: Third-Point Flexure Fatigue Apparatus (Deacon, 1965)

Around the same time that Monismith and Deacon were performing flexural fatigue tests at the University of California at Berkeley, Pell was investigating the fatigue of bituminous mixtures using a cantilevered fatigue apparatus at the University of Nottingham. The cylindrical specimens tested by Pell were typically 150 mm in length and necked down to a diameter of 31.25 mm at mid-height. The apparatus gripped the specimen at the ends, restraining the specimen from translational and rotational movement relative to the bearing, i.e., in a fixed condition. The top bearing had the ability to apply a couple which results in a uniform, pure bending moment along the unsupported length of the specimen. By oscillating the applied couple, the specimen was subjected to a sinusoidally oscillating bending moment with constant amplitude (Pell, McCarthy, & Gardner, 1961).

Similar to the researchers at the University of California at Berkeley, Pell et al. at the University of Nottingham determined that the fatigue behavior of asphalt mixtures is sensitive to variables other than simply load or displacement magnitude. In particular, the temperature and loading frequency had significant implications on the fatigue behavior. In addition to these observations, Pell et al. postulated that the critical variable in fatigue behavior is the tensile strain experienced by the bitumen and that there is a linear relationship between the log of the number of cycles to failure and the log of the applied tensile strain. This relationship became a popular means of comparing fatigue tests and is still used today.

3.1.2 Indirect Tension Tests

In the 1960's, researchers at the University of Texas at Austin started using the indirect tensile test (also referred to as the diametral test) to characterize, among other properties, the fatigue behavior of asphalt mixtures (Anagnos & Kennedy, 1983; Cowher & Kennedy, 1975). Although

several variations of the test exist, the fundamental concept is to cyclically apply a load to the circumference of a thin, cylindrical specimen along a diametral axis. The loading pattern results in a theoretically known biaxial state of stress at the center of the specimen with a compressive stress along the diametral axis perpendicular to the direction of loading and a tensile stress along the longitudinal diametral axis. The resulting deformations along and perpendicular to the loading axis are recorded by LVDT strain gauges. The test setup is shown in Figure 6.

The indirect tensile test, which was previously developed for tensile testing of concrete, gained wide-spread popularity due to its simplicity. The testing equipment is relatively inexpensive and easy to use. The specimens are simple to fabricate because they can be taken from the standard cylindrical laboratory compacted specimens. In addition to its simplicity, the test is multi-functional; the test method allows for the determination of the modulus of elasticity, Poisson's ratio, permanent deformation behavior and fatigue cracking. The major pitfall with this test as it pertains to fatigue testing is the indirect relationship itself. Fatigue is assumed to be a result of the tensile stresses and strains in the mixture. The biaxial state of stress which results from this loading pattern prohibits a direct correlation between the tensile strain in the specimen and the fatigue life of the specimen. In addition, since the loading interface is a simple bearing surface, there is no capacity for the test to induce a stress reversal. This results in the specimen undergoing significant permanent deformation during the test which in turn 'artificially' reduces the observed fatigue life.

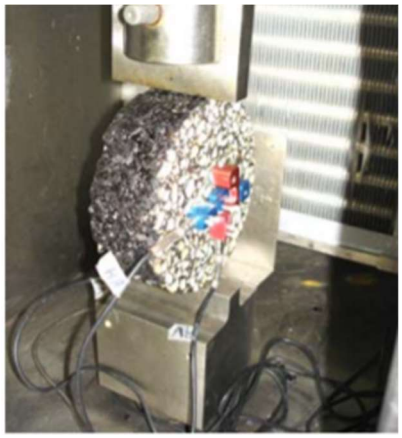

Figure 6: Indirect Tension Test (ASTM, 2017)

3.1.3 Direct Tension Fatigue Tests

Although flexural and indirect tension fatigue tests dominated the second half of the 20th century, direct axial test methods were utilized by a number of researchers at various times and locations. In 1970, Kallas utilized a test method with the capacity to apply direct tension in order to investigate the dynamic modulus of asphalt concrete in tension. The test specimens were cylinders 100 mm in diameter and 200 mm in length. Steel end caps were bonded to the cylinder using an epoxy cement. The steel caps were then connected directly to the loading apparatus (Kallas, 1970).

In 1972, Raithby and Sterling in the United Kingdom used a similar test method to investigate the fatigue behavior of asphalt concrete. The test specimens were prismatic specimens with 75-mm square cross-sections and 225-mm long (Raithby & Sterling, 1972). These studies provided valuable information on the effect of load shapes and rest periods on the fatigue performance of asphalt. The tests also demonstrated the potential for performing complete fatigue tests via uniaxial loading. This particular test utilized specialized equipment and the relatively large

specimens were cut from a compacted asphalt mat – a rather atypical laboratory procedure. As such, the test method did not gain much popularity elsewhere.

In 1990, Kim, along with various other researchers at North Carolina State University, began research on the application of continuum damage for modeling the behavior of asphalt as it relates to damage. The general concept of this approach is to separate the effects of viscoelasticity and damage. For purely elastic materials, this task is fairly straightforward. Since for these materials the stress-strain relationship is not time-dependent, damage can simply be interpreted as the deterioration of the materials modulus of elasticity. However, for viscoelastic materials, such as asphalt concrete, the stress-strain relationship is time-dependent. As such, the current stiffness of the material depends on both current and past stress-strain states. The change in the material's stiffness over time is thus a result of both damage and viscoelastic effects. In order to understand the accumulation of damage within the material, the two effects must be uncoupled. Schapery developed a method of doing just that through the use of pseudo strain. The theory for this approach is covered in the literature (Schapery, 1984). In short, the standard linear viscoelastic stress-strain relationship is replaced with a linear elastic relationship through the use of an elastic-viscoelastic correspondence principle which takes into account the hereditary effects via a convolution integral.

The focus of Kim's research was adopting Schapery's correspondence principle approach for the uniaxial modeling of asphalt concrete. The study revealed that such an approach could indeed be used to accurately model and predict the response of asphalt to various loading histories (Kim & Little, 1990). This marked the beginning of a significant breakthrough in the study of the behavior of asphalt. Up to that time, the majority of fatigue studies consisted of comparing the

performance of different asphalt mixes subjected to fatigue loading and determining a correlation between fatigue lives determined in the laboratory versus that observed in the field. The potential for accurately modeling and predicting fatigue behavior resulted in a significant amount of research focusing on this technique. Furthermore, since the technique was found to be compatible with uniaxial modeling, the uniaxial direct tension test began gaining popularity accordingly.

In the initial study mentioned previously, Kim and Little (Kim & Little, 1990) used a testing machine made up of two adjacent plates. Beam specimens similar to those typically tested in flexure were attached at the ends via epoxy to the plates. The beam's longitudinal axis was oriented perpendicular to the joint between the plates. To perform the test, one plate remained fixed while the other underwent controlled movement. As the research continued, the laboratory tests used to validate the modeling evolved to a direct tension, constant strain-rate elongation test performed on cylindrical test specimens (Park et al., 1996).The fabrication process involved compacting asphalt slabs via the rolling wheel compaction method. Sample cylinders with a diameter of 102 mm and a length of 203 mm were cored from the compacted slabs. To perform the test, the specimen ends were glued to end plates which were in turn connected to the loading apparatus, much like the previously discussed test procedure used by Kallas.

Around the same time Kim was applying the continuum damage approach to asphalt mixtures, the Strategic Highway Research Program (SHRP) was created to develop new techniques and equipment to improve the design and construction of pavements. The primary result of the program was a new HMA mix design method, called Superpave (Asphalt Institute, 1996). In terms of asphalt testing and, in particular, uniaxial testing, a key outcome from this extensive

study was the National Cooperative Highway Research Program (NCHRP) Projects 9-19 (Witzcak, 2002) and later 9-29 (Bonaquist, 2008) which resulted in the development of the AMPT. This versatile testing machine was created with the intent for labs to be able to perform various mechanical tests on asphalt mixtures cored from Superpave gyratory compacted cylinders. As a result, a majority of test procedures developed after this time were created to be compatible with the AMPT using test specimens which can be cut or cored from the Superpave gyratory compacted cylinders.

AASHTO Provisional Standard TP107 provides a standard method for performing a uniaxial, tensile fatigue test on cylindrical asphalt specimens to determine the damage characteristic curve for an asphalt mixture. An overview of this method is provided in section *2.1 Background.* The damage characteristic curve is a product of the continuum damage model developed by Kim et al. Simply put, the characteristic curve determines the amount of damage accumulated by an asphalt mixture based on a set of assumed conditions, such as frequency, temperature, etc. Beyond this provisional standard, uniaxial fatigue tests remain a rather customized procedure with the exact approach specified according to the intent of the study. However, due to the development of the AMPT, most tests follow the same core concept. Cylinders are cored from gyratory compacted specimens and the ends are bonded to circular steel loading plates which can be attached directly to the AMPT. For stress-controlled tests, the specimens are subjected to cyclic loading of pure tension or tension-compression with a constant load amplitude. Crosshead-controlled tests apply cyclic actuator displacements with constant displacement amplitude.

3.2 Fatigue Failure Criteria

As mentioned previously, there is no single, all-encompassing definition of failure in an asphalt fatigue test. As new fatigue test methods developed, so too do various fatigue failure criteria. This section offers a brief overview of frequently used failure criteria.

Perhaps the simplest definition of failure is the complete fracture of a specimen across the entire cross-section. The advantage of such a definition is that there is little room for subjectivity in determining when the failure occurred. This failure criterion is also attractive in a practical sense; the pavement is considered acceptable until it fractures. While this concept works well for stress-controlled tests, complete fracture is less desirable for strain-controlled tests. In a stress-controlled test, the applied load amplitude remains constant. This results in a relatively rapid fracture process once macro-cracks begin to form. Conversely, for a strain-controlled test, the load amplitude diminishes as the resistance of the specimen deteriorates. This results in a nearly asymptotic approach to complete fracture, and thus a tediously drawn-out fracture process. This phenomenon was observed early on by Pell (Pell et al., 1961):

> "With bituminous mixes in the 'constant stress' tests the initiation of a crack appears to be followed by immediate and catastrophic failure of the specimen which causes the machine to stop, whereas the measurement of fatigue life in the constant strain machine is dependent on the propagation of a crack across a strip of conducting paint."

A more commonly used failure criterion is the reduction of the material's stiffness to some pre-defined ratio of its initial value. The traditional definition of failure in fatigue testing of asphalt is the cycle at which the specimen's stiffness reduces from its initial stiffness by 50%. Since this does not require the complete fracture of the specimen, this definition yields a significantly faster test which allows for the accumulation of more data. In addition, the physical meaning of this

failure definition is simple, therefore the results of a test are directly relatable to the expected performance of a mixture in the field; a mixture that reduces to 50% initial stiffness quickly relative to other mixtures under the same conditions is expected to be less capable of resisting damage due to fatigue than said other mixtures.

A major disadvantage with this failure criterion is its inability to measure the remaining service life of a mixture. Fatigue cracking is generally understood to be the result of microcracks forming and propagating as a result of fatigue loading until they eventually coalesce into macrocracks. Until this occurs, there is no cause for the pavement to be deemed unacceptable, at least with respect to fatigue. This 50% reduction is not a consistent estimator for how long the pavement can continue to perform at an acceptable level. In terms of remaining service life, the selection of a 50% reduction in stiffness representing failure is a rather arbitrary criterion. This arbitrary criterion is compounded by the fact that the 50% reduction in stiffness is relative to an initial stiffness that is taken at an arbitrarily selected early cycle. The first several cycles in a cyclic test experience a significant amount of variation in loading rate administered by the servo-hydraulic machine prior to achieving a 'smooth' actuator movement. The stiffness calculated during these first few cycles does not represent the stiffness of the mixture under the assumed loading pattern, therefore the 'initial' stiffness must be taken after a number of initial cycles, e.g., 200 cycles or 20 seconds. As such, this criterion for failure, though useful in comparing the fatigue performance of asphalt mixtures prior to failure, cannot be used to compare the fatigue behavior of asphalt throughout its entire potential service life. This concept is illustrated in Figure 7 below. The stiffness reduction throughout the course of two tests is shown. These were controlled-crosshead displacement uniaxial cyclic fatigue tests. Each test resulted in similar

initial strains. The number of cycles to a 50% reduction in stiffness for each test are also similar at about 67,000 cycles. Note, however, that the remaining number of cycles to the rapid decrease in stiffness, an indicator of macrocrack formation, are very different in the two tests.

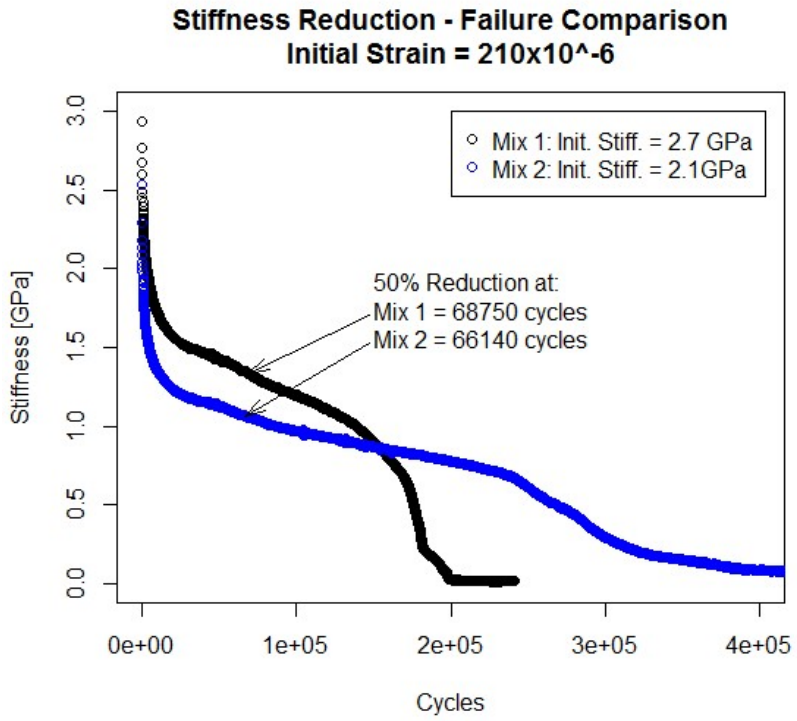

Figure 7: Comparison of 50% Stiffness Reduction for Two Tests

During both stress-controlled and strain-controlled cyclic fatigue tests, the test specimen typically undergoes three phases with respect to the stiffness of the material. During the initial phase the stiffness rapidly decreases at a decreasing rate. After some number of cycles, this reduction reaches an approximately constant slope. Finally, the third stage occurs when the stiffness begins to decrease at an increasing rate until it eventually approaches zero stiffness. Over the last two decades, researchers have been focusing on failure criteria on this third stage. This approach better represents failure in terms of the material reaching unacceptable performance levels.

One such failure criterion that received a significant amount of popularity was proposed by Reese at the California Department of Transportation. Reese postulated that this rapid loss in stiffness was marked by a sudden change in direction of the slope of the phase angle, and the cycle at which this occurs should be considered failure (Reese, 1997). This is illustrated in Figure 8. Ghuzlan and Carpenter took a similar approach, but focused on the dissipated energy ratio, rather than the phase angle (Ghuzlan & Carpenter, 2006). The dissipated energy ratio (DER) is defined as the difference in energy dissipated by one cycle and that by the next cycle, divided by the energy dissipated in that cycle,

$$DER = \frac{E_{i+1} - E_i}{E_i}$$

where,

E_i = energy dissipated during cycle i

The energy dissipated in one cycle can be determined by the equation

$$E_i = \sigma_i * \epsilon_i * \pi * \sin(\theta_i)$$

where

σ_i = peak stress magnitude during cycle i

ϵ_i = peak strain magnitude during cycle i

θ_i = phase angle during cycle i

The failure criterion proposed by Ghuzlan and Carpenter defines failure as the point at which the DER begins to rapidly increase away from a previously reached plateau valley. This concept was expanded upon by Sabouri for application in the previously mentioned continuum damage model. Essentially, the dissipated energy is converted to a dissipated pseudo energy by means of

the elastic-viscoelastic correspondence principle, and then a relationship is determined between the rate of pseudo energy release and fatigue life. This criterion can then be applied to the continuum damage model for prediction of fatigue failure (Sabouri, 2014).

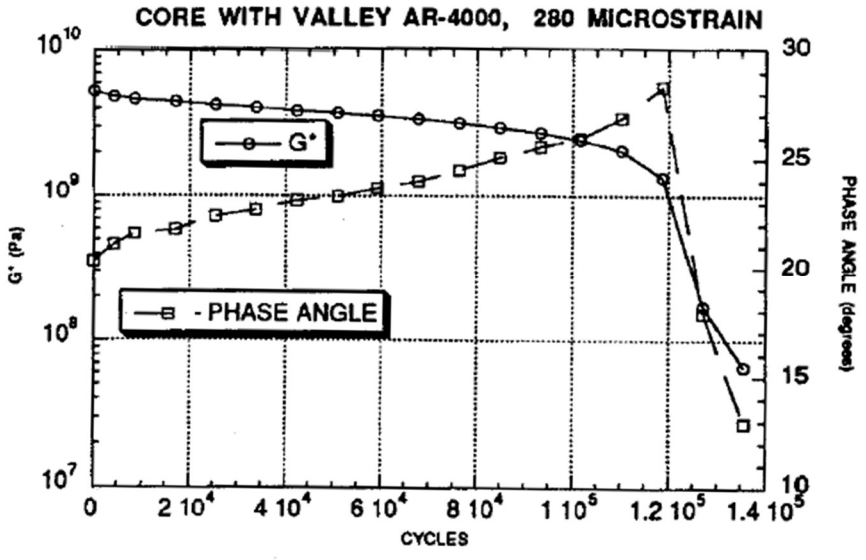

Figure 8: Rapid Change in Phase Angle as a Failure Criterion as Proposed by Reese (Reese, 1997)

3.3 Recent Developments Addressing Uniaxial Fatigue Challenges

This study focuses on two primary challenges associated with current uniaxial fatigue testing of asphalt. The first is the occurrence of end failures, that is macrocracks that form outside the gauge length of the LVDTs. End failures render the test results essentially useless, and, as a result, test procedures should be developed to avoid end failures if at all possible. A detailed description of possible causes for end failures is provided in section *2.2.1 End Failure.* The other primary challenge is the testing of asphalt concrete samples cored from the field. The majority of simple performance tests use 150-mm long cylinders cored from a gyratory compacted cylinder. However, most pavements are constructed in lifts less than 150-mm high. This means that a sample cylinder cored from the field will typically have more than one lift included in it and, as

such, cannot be used to test the performance of that mixture. There have been a number of studies which have attempted to address these challenges.

Since the early days of fatigue testing of asphalt, there have been studies which have intentionally altered the geometry of the test specimen in order to ensure failures within the middle of the specimen where the deformations are being monitored. At the University of Nottingham in the early 1960s, Pell began research on the fatigue testing of asphalt concrete. The test specimens used in this study were cylindrical with a diameter that continuously tapered from the ends to the middle. The minimum diameter at the middle of the specimens were 31.25 mm. The specimens were fabricated using a split mold and compacted with a combination of tamping by hand and hydraulic press.

Researchers at Delft University of Technology utilized a specimen geometry with a tapered cross-section, similar to that used by Pell. The procedure involves using a split mold during compaction to produce a 90-mm long, parabolically tapered cylinder with 80-mm diameter at the ends and 50-mm diameter at the center. The split mold is inserted into a gyratory compaction mold and compacted in the same way as a typical gyratory compacted cylinder. According to the report, the tests performed on these specimens all resulted with mid-failures within the gauge points (Erkens & Poot, 2001). This indicates that tapering the cross-section of an asphalt specimen for tensile testing encourages the failure zone to develop near the middle and within the gauge length of the LVDTs. The major drawback of this procedure is its incompatibility with standard SPT equipment and procedures. In addition, such a geometry would be difficult to achieve for specimens cored from the field.

Recently, a team of researchers performed a study to determine potential methods of addressing the issue of testing field samples in fatigue (Kutay, Gibson, Youtcheff, & Dongré, 2009). The study proposed using cylinders with a diameter of 38.1-mm and height of 100-mm. The modified dimensions would allow for cylinders to be horizontally cored from field samples with as little as 50-mm thickness. Testing of these horizontal cores also better represents the tensile strains at the bottom of the asphalt concrete experienced in the field, since these tensile strains primarily occur laterally near the bottom due to flexure. The resulting damage characteristic curves display little to no change between the standard size and the reduced size. The study was expanded in an NCHRP IDEA Project by a team at North Carolina State University. The project confirmed the finding that damage characteristic curves are similar between small and large diameter cylinders, however the dynamic modulus of small cylinders varied significantly at higher temperatures. This result is encouraging, as it suggests that test specimen dimensions smaller than the standard representative volume element (RVE) dimensions are possible without biasing fatigue test results. The challenge of end failures was still evident during these tests, however. Indeed, the occurrence of end failures was quite high for cylinders cored horizontally due to the high air void content at the edges of the cylinder, therefore the team suggests coring vertically from laboratory compacted cylinders (Castorena, Kim, Pape, & Lee, 2017).

Another example of a possible method to overcome the challenge of testing field samples is the Overlay Tester. A team of researchers at Texas A&M University and the Texas Department of Transportation recently studied the potential of using the Overlay Tester as a measure of evaluating fatigue performance of asphalt mixtures. The Overlay Tester is a test method developed to measure a material's ability to resist reflective cracking. The test involves bonding

a 38 mm high by 75 mm wide by 150 mm long specimen to two separate, adjacent loading plates. One plate is held fixed while the other is moved laterally in a cyclic, displacement-controlled manner. The dimensions of the specimen are such that it can be fabricated from a standard Superpave gyratory compacted cylinder as well as specimens cored from the field. The research team found a correlation between the number of cycles to failure from the Overlay Tester method, standard beam fatigue testing and observed field performance. As such, the Overlay Tester was suggested as an SPT option for fatigue performance testing (Zhou, Hu, Chen, & Scullion, 2007). One challenge with this test is the non-uniform stress distribution. The specimen is bonded along a surface parallel to the direction of loading and offset from the center. This results in a highly non-uniform stress and strain distribution across the cross section of the specimen and, as such, the results are difficult to use in conventional analysis. This test method is illustrated in

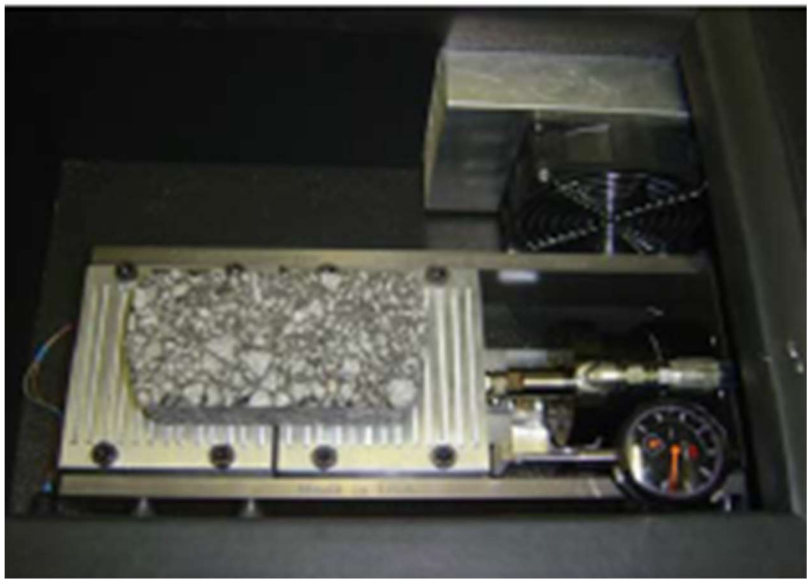

Figure 9: Overlay Tester (Zhou et al., 2007)

As described in detail in section *2.2.1 End Failure,* Archilla discovered that cyclic fatigue testing at 40°C resulted in a high number of end failures very close to the loading platens (A. Archilla & Corrales-Azofeifa, 2017). The tests were stress-controlled and the specimens tested were the standard SPT cylinders cored from gyratory compacted specimens. In an attempt to reduce the frequency of these end failures without modifying the compaction process or the testing equipment, Archilla investigated the possibility of trimming the specimens post-compaction to reduce the cross-section. The new specimen geometry reduced the diameter from 100-mm at the ends to 90-mm in the middle. The 10-mm reduction was achieved in a staircase pattern over a length of 20-mm, resulting in a constant diameter of 90-mm over the middle 110-mm versus a total length of 150-mm. The staircase pattern was smoothed with epoxy cement in order to avoid failure at the strain concentrations located at the discontinuities formed by the staircase pattern. This modified specimen geometry drastically improved the occurrence of middle failures. Indeed, all specimens tested thus far meeting these modified test specifications have resulted in middle failures. The results are shown in Figure 10.

Figure 10: Modified 'Dogbone' Shape Specimens with Middle Failures (A. Archilla & Corrales-Azofeifa, 2017)

3.4 Summary

Over the last 50 years, there has been a significant amount of progress made towards understanding the fatigue behavior of asphalt. Despite this progress, there is still a need for a

practical, reliable, standardized test to characterize the fatigue performance of asphalt mixtures. The literature review demonstrates the various tests that have been developed during different studies and offers a glimpse of the advantages and disadvantages of each method. The review also demonstrates the emergence of the uniaxial, cyclic fatigue testing as a potential Simple Performance Tester for the purpose of characterizing fatigue behavior. However, as discussed in detail in section *2.2 Motivation for Study*, there are challenges involved with this test that must be addressed in order for its maximum potential to be achieved. Two primary challenges are the occurrence of end failures and the applicability of the test to field samples. The following chapter proposes a modified test specimen geometry to address these challenges.

CHAPTER 4: DEVELOPMENT OF A THIN SPECIMEN WITH TAPERED CROSS-SECTION FOR FATIGUE TESTING

4.1 Development of New Specimen Geometry

The objective of this study was to develop a specimen configuration for fatigue testing of asphalt mixtures that would reduce the frequency of end failures and enable the testing of field samples paved in thin lifts. The following sections discuss why the proposed geometry was selected.

4.1.1 Key Factors Influencing Specimen Geometry

Perhaps the most important objective in the development of the new geometry is a tapered cross-section at the middle. End failures have been attributed to the higher air void content near the ends as a result of the gyratory compaction process. However, as discussed in section *2.2.1 End Failure*, a uniform cross section along the depth of the longitudinal axis would theoretically only result in a frequency of middle failures equal to the ratio of the gauge length to the overall specimen length on average. Additionally, the specimen must be gripped at the ends in order to develop a tensile stress. This grip, typically achieved via some form of bonding agent, leads to strain concentrations at this interface which encourages end failures. It is therefore of paramount importance that the cross-section of the specimen in the region of interest (between the gauge points) be sufficiently reduced to ensure the critical strains occur in this region.

Another important consideration in the development of the new geometry is its compatibility with samples cored from the field. Asphalt pavements are typically constructed in lifts of 75-150 mm. In some cases, such as thin lift overlays, the lifts can be as thin as 19 mm though they are often between 25 and 38 mm. As such, the new test specimen geometry must have one

orthogonal dimension less than the minimum expected lift thickness (of course, this is not possible for 19 mm lifts but it can be achieved for slightly thicker lifts).

Finally, it is imperative that the proposed specimen be compatible with standard laboratory procedures. As discussed in the literature review, there have been multiple examples of researchers using a split mold during compaction to achieve a customized geometry. While this method lends itself well to tapering the cross-section, the use of a split mold is not a standard process employed by most pavement laboratories. It is also unclear how uniform the resulting air void distribution is for this method of compaction since this is difficult to achieve even for cylindrical specimens with the SGC. Furthermore, the standard Superpave gyratory compactor was designed with the intent of simulating the compaction process used in the field. It is unclear whether the use of a split mold achieves this same representation. Therefore, the proposed specimen geometry should be obtainable from a standard Superpave gyratory compacted cylinder. In addition to compatibility with standard compaction processes, the specimen should be compatible with standard testing equipment. As previously discussed, the AMPT has emerged as the standard method of testing asphalt mixtures for performance evaluation. As such, the dimensions of the proposed geometry should be such that the specimen can be attached to and tested by the AMPT.

4.1.2 Proposed Specimen Geometry

The previous section discussed the factors influencing the proposed test specimen geometry. Considering all these factors, the proposed specimen geometry is a 110-mm by 100-mm rectangle sliced horizontally from the middle of a 150-mm diameter gyratory compacted cylinder. The longer sides are tapered at a radius of 175-mm over a length of 90-mm to a width

of 88-mm at mid-height. The thickness of the specimen can be varied, with a preferred thickness of 38-mm to provide a cross section large enough to accommodate larger aggregates and thus minimize the effects that few particles may have on the test. The specimen is then subjected to uniaxial loading along the longer axis. A schematic of the proposed geometry is shown in Figure 11. It should be noted that these dimensions have been refined over the course of the study. In developing the new specimen geometry and associated production procedures, the dimensions varied from specimen to specimen, particularly in the early stages. The dimensions listed here have been found to be ideal based on experience and will be specified for future experimental work.

The dimensions of the rectangle were selected to fall within the circumference of a 150-mm diameter circle. In this way, the rectangle can be cut from a slice taken from a gyratory compacted cylinder as depicted in Figure 12. The thickness of the slice can be selected at the user's discretion, however a thickness of 25-mm and later 38-mm were the standard thicknesses used during this study. These dimensions achieve a 2:1 ratio for minimum dimension to nominal maximum aggregate size (NMAS) for mixtures with NMAS of 12.5-mm and 19-mm respectively. This thickness also allows for one gyratory compacted specimen to yield multiple test specimens, even after removing a portion of each end from the cylinder to obtain a representative volume. A thickness greater than 38-mm would result in a portion of the asphalt overhanging the circumference of the loading platens used in SPT testing.

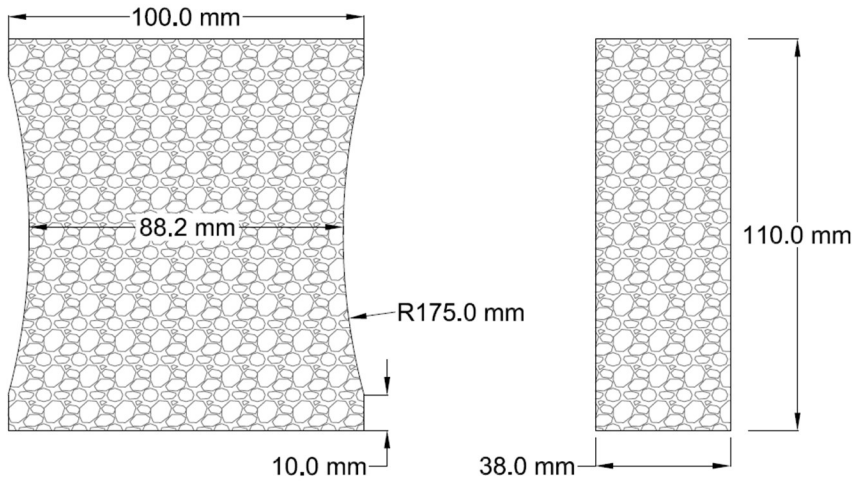

Figure 11: Proposed Specimen Geometry

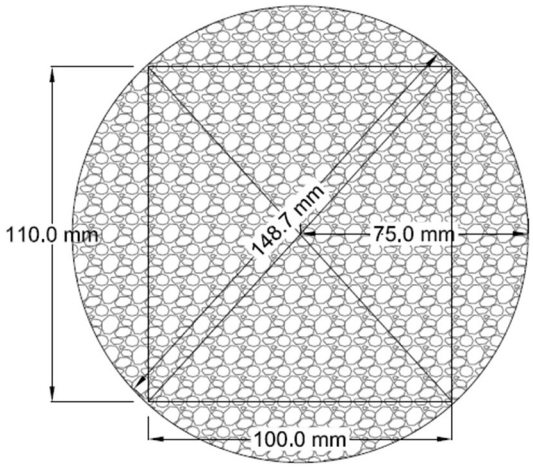

Figure 12: Dimensions of Rectangular Slice Within Original Cylinder Circumference

The specimens are created from the gyratory compacted cylinder using a saw with diamond cutting edges as is standard practice in trimming the ends of SPT cylinders. The process of producing the final specimens includes cutting the compacted cylinder into horizontal slices (discarding the two end slices), cutting the edges to yield the rectangular shape, then trimming the longitudinal sides to yield the 175-mm radius arc. The first two cutting procedures are relatively straight forward, as they involve straight cuts in the direction of the blade. The trimming of the arc is a more refined process. The cut is achieved by utilizing a jig with an arced

back to glide the specimen about the blade. The geometric layout of this jig is illustrated in Figure 13. The jig used during this study was created with acrylic. A more detailed description of each step in the procedure is included in section *4.2 Specimen Preparation.*

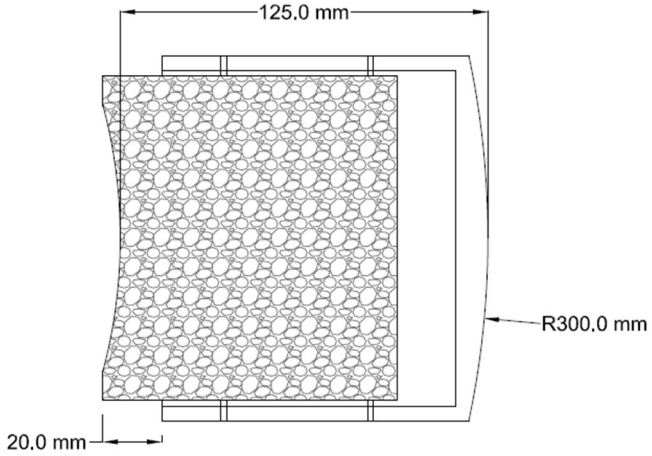

Figure 13: Arc Trimming Jig Geometry

With the exception of the trimming jig, which is relatively cheap and simple to create, no specialized equipment is required to produce these specimens. The trimming procedure involves a learning curve as the lateral cut is rather unique. However, once the technique is understood, the fabrication process to create 2 or 3 specimens from 1 compacted cylinder takes between 1 to 2 hours. A significant portion of this time includes the set-up process. If three cylinders are prepared, the process can produce 6-9 specimens in 4 hours or less. Therefore, despite the added cutting procedures, the fact that one compacted cylinder can yield multiple test specimens, coupled with the fact that there is no need to core, results in the time required per specimen to be comparable to that of the SPT test cylinders.

4.1.3 Intermediate Material

One challenge with this specimen geometry is the reduced length as compared to the SPT test cylinders. Recall that the AMPT was designed to test cylinders with a length of 150 mm with

steel loading platens on each end. The proposed specimen length is 110-mm long and thus beyond the recommended range of the actuator ram in a standard AMPT machine. This requires an intermediate material to be added between the loading platens and the test specimen. Although this initially appears to be a hindrance, the addition of material between the loading platens and the steel plates offers an advantage. It has been discussed previously that the lateral restraint enforced at the ends by the bonding agent causes strain concentrations at the interface. This is due to the differences in modulus between the steel loading platens and the asphalt mixture. By adding an intermediate material between the steel and asphalt with a modulus similar to that of asphalt, the differential lateral strains, and thus the concentration effect, at the ends of the specimen is reduced.

Phenolic linen was selected as the material to use at the interface. Phenolic linen has a modulus of 8390 MPa at 20°C. The linen can be ordered in pre-fabricated blocks. The blocks used in this study were cut to a size of 105-mm long by 45-mm wide by 16.33-mm thick. The length was selected to match the diameter of the loading platen at the center. The width was selected to match the 38-mm specimen thickness with sufficient room on each side to allow for a fillet in the steel putty (this was found to increase the grip strength). The thickness of the blocks was selected to result in a total plate-to-plate length of approximately 150-mm including bonding thicknesses at the interfaces. When bought in bulk (100 blocks) the cost of the phenolic linen was approximately $3.00 per block.

4.1.4 Finite Element Analysis Verification (Linear-Elastic)

The proposed specimen geometry was conceptualized by Archilla as an extension of the tapered cylindrical specimen developed previously (A. Archilla & Corrales-Azofeifa, 2017). The tapered

cross-section showed promise for alleviating the end failure challenge based on both experimental and analytical results. The fabrication process of the tapered cylindrical specimens was tedious, however, and the test did not allow for the testing of thin lift pavements. This gave rise to the idea of using the horizontal slices with a continuously tapered cross-section to facilitate a simpler fabrication process. The subsequent question was: at what radius should the cross-section be tapered to yield a favorable strain distribution? Too small of a radius would result in a steep taper and consequently with substantially non-uniform stress distributions across vertical and horizontal cross-sections. Too large of a radius would not reduce the cross-section sufficiently to force the critical strains to occur in the middle.

A finite element analysis was performed to determine the optimal radius and taper length. The analysis was simplified to a static, linear elastic scenario. While this is an oversimplification for determining accurate stress and strain magnitudes, the purpose of the analysis was solely to determine the relative distribution of strains at the middle compared to the ends as well as the uniformity of the strain distribution across the cross-section within the gauge length. Therefore, the static, linear analysis was deemed sufficient for determining these optimal dimensions.

Table 1 illustrates the relevant mechanical properties assumed for each of the materials used in analysis. The modulus and Poisson's ratio used for asphalt were selected to match the observed values at 40°C since the strain concentration problem is more pronounced at higher temperatures. The load applied during the simulation was selected to result in a nominal strain of 100 με (i.e., 10^{-6} mm/mm). The resulting strain distribution is shown in Figure 14. As shown, the specified geometry results in a nearly uniform strain distribution within the middle 70-mm of the specimen. The strain concentration at the ends are still evident due to the lateral confinement.

However, the strain magnitude is greatest in the middle, implying that this geometry will result in failure in the middle prior to end failures. The strain at mid-depth varies from approximately 107% at the edges to 93% in the middle with respect to nominal strain. A more detailed finite element analysis is required to better understand correction factors required when analyzing test results to account for slight non-uniformity in the strain distribution between the gauge points.

Table 1: Mechanical Properties of Materials Used in FEA

	Stiffness Modulus (MPa)	Poisson's Ratio
Steel Platens	193000	0.28
Steel Putty (Bonding Agent)	5860	0.32
Phenolic Linen	8390	0.32
Asphalt Mixture	690	0.4

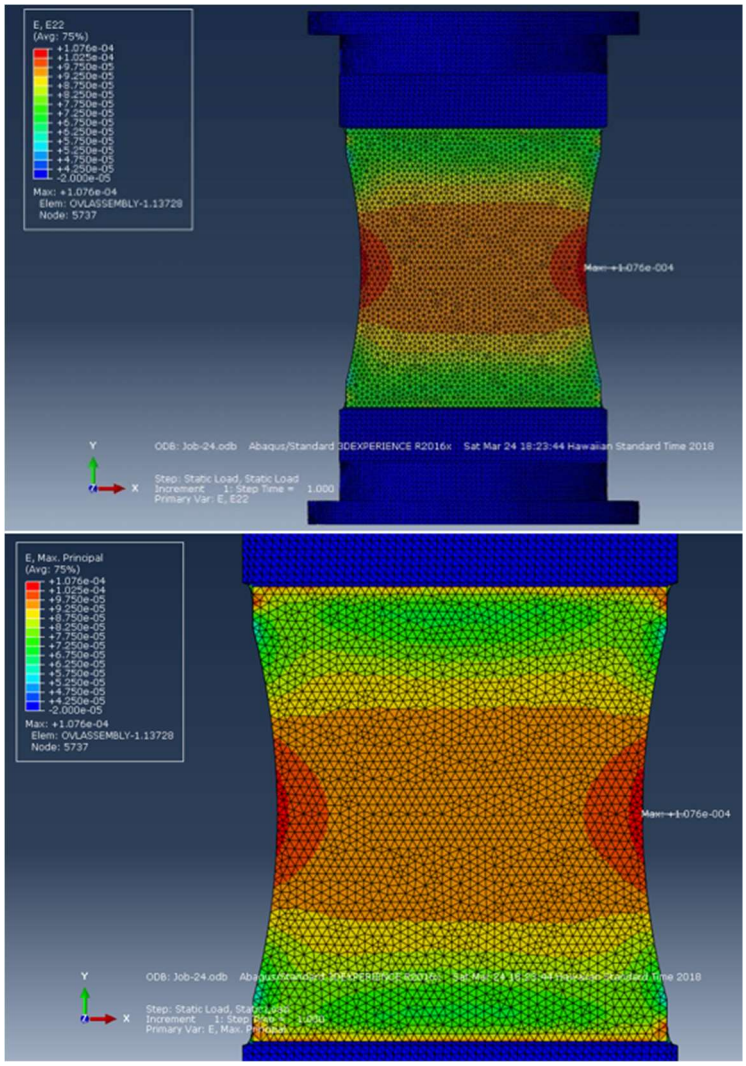

Figure 14: Strain Distribution from Static, Linear-Elastic Finite Element Analysis of Proposed Test Specimen: Vertical strain distribution (top); Principal Tensile strain distribution.

4.2 Specimen Preparation

Producing specimens with the proposed geometry involves three phases after compaction of the cylinders: slicing the compacted cylinders into discs with the desired test specimen thickness, cutting the discs into a 100-mm by 110-mm rectangle, and trimming arcs from the 110-mm sides. The following sections describe in detail the process for these three steps.

4.3.1 'Slices' from the Compacted Specimen

For this study, sample cylinders were mixed and compacted per AASHTO T312 which utilizes the Superpave gyratory compaction process (AASHTO, 2016). This process produces cylinders with a diameter of 150-mm and a variable height which can be specified to yield a target air void content (see section *4.3 Target Air Void Content*). Once the cylinders are compacted, they must be sliced into discs with a thickness equal to the desired thickness of the final test specimens. Cutting asphalt cylinders perpendicular to the longitudinal axis is a standard process because SPT cylinders cored from gyratory compacted cylinders are trimmed at the ends to produce flat parallel loading surfaces. Gyratory compacted cylinders have higher air void content at the ends, so this process also removes these undesirable segments.

The cutting procedure uses a circular saw with a diamond edge blade to perform the cut. The specimen is supported by a surface that is free to move parallel to the axis of the blade. Standard SPT cylinders are approximately 100-mm in diameter. This allows for a 250-mm diameter blade to cut a cylinder in one pass. When trying to cut the full, 150-mm diameter compacted cylinder, however, a 400-mm diameter saw is required to perform the cut in one pass. A 400-mm saw capable of performing 'precise' cuts was unavailable during the course of this study and is less common in typical pavement labs.

To overcome this challenge, the cylinders are sliced in multiple passes. Wood blocks with perpendicular edges are used to control the thickness of the cut. One edge of the block is placed on the cutting platform parallel to the blade at a distance equal to the desired thickness of the cut. The adjacent edge of the block is set flush to the back support of the platform. The cylinder is then placed with one face flush to the wooden block and the side flush with the back support.

Once secured, slight pressure is applied from the opposite end of the cylinder to ensure contact with the wooden block for the entirety of the cut. A cut is made as deep as possible without making contact with the blade's central support. The cylinder is then pulled back and rotated 120°. This process is repeated three times until a complete cut is made. The cutting procedure can be seen in Figure 15. While this procedure has yielded good results thus far, achieving the cut in one pass with a 400-mm diameter blade is clearly a more efficient and accurate means of performing the cut and is the recommended method.

Figure 15: Procedure for Cutting Discs from a Compacted Cylinder

4.3.2 Rectangular Specimens from the Discs

Once the discs have been cut from the cylinder, they must be cut into a 100-mm by 110-mm rectangular specimens. Using a tracing template, the discs are marked to indicate where the cuts should be made. An important factor in the production of these test specimens is the perpendicularity of cuts to adjacent edges. Non-perpendicular sides will result in eccentric

loading while performing the test, which can affect the results. If the eccentricity is significant, it may even cause the steel putty to fail resulting in a wasted test specimen. For this reason, an additional platform was created from acrylic with 4 set screws, one in each corner. The screws can be tightened or loosened to raise or lower a corner. This allows for adjustments to be made if it is found that the blade is not perfectly perpendicular to the cutting platform. This can happen if the blade becomes slightly warped after extended use. The procedure and set up for cutting the rectangles from the discs is shown in Figure 16.

It is important to note that the markings are used to understand where to start the cut in order to achieve the required dimensions. They should not be used to indicate a perpendicular cut. The perpendicularity of two adjacent cuts is enforced by the perpendicularity between the back support and the blade. Attempting to use the markings as a guide while cutting will result in imperfect perpendicularity. Once the rectangular specimen has been cut, the dimensions should be verified. Based on experience, the specimen can be deemed acceptable if the lengths of opposite sides are within 1-mm of one another, although ideally this difference is less than 0.25-mm. A small eccentricity developed due to the lack of parallelism can be offset to a certain degree through the use of set-screws between the top platen and the top plate of the load cell. This is explained in more detail in section 5.2.1.3 Installing the Specimen in the AMPT.

Figure 16: Procedure for Cutting Rectangular Specimens from Discs

4.3.3 Trimming the Rectangular Specimens

Once the rectangular specimens have been cut and approved, the longitudinal sides must be trimmed to produce the arc. A jig is used to produce this cut. The geometry of the jig was shown previously in Figure 13. The actual set up is shown in Figure 17. The concept is to cut the specimen by moving the specimen laterally about the blade which is in a fixed position. The depth of the cut is varied as the specimen moves laterally, creating the arc. This is achieved by gliding the jig along the back support which has a radius equal to the back edge of the jig. The jig has an opening width of approximately 115-mm to account for rectangular specimens with longitudinal edges slightly longer than 110-mm. There are set screws on both ends of the jig to lock the specimen in place within the jig. Aluminum shims should be placed between the set screw and the specimen to avoid damaging the specimen.

The proper set-up of the saw and supports is critical to achieving a successful cut. The first variable to account for is where the specimen meets the blade vertically. Prior to trimming, the edge being cut is flat. This means that the blade touches the edge at a single point. Ideally, the specimen should be raised as high as possible without touching the blade guard. The specimen can be raised by adding flat platforms on top of the cutting platform. An additional surface oriented vertically must be added behind the platforms to serve as a back support. Even with this vertical adjustment, the blade will touch the specimen edge above mid-depth, resulting in a cut that varies in depth along the thickness of the specimen. To account for this, the specimen is trimmed, flipped, then trimmed again. This results in a slight ridge at the center of the specimen. The closer the edge is to being tangent with the blade, the less pronounced the ridge. This concept is demonstrated by the left image of Figure 17.

After the vertical alignment is set, the lateral positioning of the jig and specimen must be centered. To accomplish this, the back support of the jig is positioned such that its centerline is parallel to and in line with the blade. Likewise, since the opening in the jig is slightly larger than the length of the specimen, the center of the specimen must be positioned within the jig such that its centerline lines up with the blade and the centerline of the back support. This position is then fixed by the set screws and aluminum shims.

Finally, the longitudinal alignment must be set by fixing the distance the platform can be moved into the blade. Recall from Figure 13 that the proposed geometry of the arc includes a chord length of 90-mm and a radius of 175-mm, resulting in a cut depth of approximately 6-mm. The radius of the back support is fixed; therefore, the operator has control only of how far the specimen is allowed to move in the direction of the blade, i.e., the depth of the cut. The objective

then, is to control the cut depth such that the cut is 6-mm deep at the center of the specimen and 0-mm deep at 10-mm from each edge. This is enforced by setting a ‘brake’ on the cutting platform tracks. The ‘brake’ is simply a strip of metal that is clamped to the track that prevents the platform from rolling beyond a certain point. To set the longitudinal alignment, the operator, after fixing the specimen within the jig, moves the specimen forward and laterally until it rests on the blade at a distance of 10-mm from an edge. The operator then sets the brake with the platform in this position so that the platform can be rolled back from that position but not past it. As a final check, the specimen is moved laterally to the other side of the jig to ensure that, as the jig glides along the back support, the first contact with the blade is made at 10-mm from the edge. This will confirm the lateral and longitudinal alignments are set properly.

Once the set-up is complete, the specimen is ready to be trimmed. The trimming process involves gliding the specimen along the back support to perform a lateral cut perpendicular to the blade. As the jig is moved laterally, pressure is applied in two directions, tangentially along the back support and radially between the jig and back support. With one hand, pressure is applied perpendicular to one side of the jig to cause a tangential movement along the back support. This movement combined with the rotation of the blade is what trims the specimen. With the other hand, the jig is held flush against the back support to ensure the cuts do not go deeper than intended. The cut must be performed slowly, trimming only one or two millimeters deep at a time. Attempting to cut too much material at a time will result in warping of the blade. It will also be difficult to perform a smooth movement along the arc which will result in discontinuities and thus an unacceptable cut.

Figure 17: Arc Trimming Jig and Set-Up in Profile View (Left) and Plan View (Right)

Figure 18: Specimen Shape After Cutting

Performing all the necessary cuts will result in a specimen such as the one shown in Figure 18. Once all the cuts have been completed, the dimensions of the specimen should be measured and recorded. The dimensions specified in Figure 11 are the ideal geometry. However, due to the number of cuts that must be performed and potential for human error, producing a specimen with

the exact dimensions is difficult. As the process is refined, the objective will be to develop equipment to minimize the reliance on operator precision. Until this time, however, it is to be expected that cut dimensions will vary slightly from the idealized geometry. What is more important is the accurate recording of the final dimensions and verification of perpendicular edges. If any opposite faces are found to have dimensions that vary by more than 1-mm, or if any adjacent edges vary noticeably from 90°, corrective trimming should be attempted. If correction is not feasible, the specimen should be discarded as it will result in eccentric loading and thus a non-uniform stress distribution.

4.3 Target Air Void Content

Air void content is one of the key variables affecting the performance of asphalt concrete. Understanding the air void content of test specimens is critical for proper analysis. Air void content is derived from the measurement of two specific gravities: the bulk specific gravity of the compacted specimen (AASHTO T-166) and the maximum theoretical specific gravity of the same mix (AASHTO T-209). From a volumetric analysis, it can be shown that the air void content is simply the remainder of 1 less the ratio of the bulk specific gravity of a specimen to the maximum specific gravity of that mixture:

$$AV = \left(1 - \frac{G_{mb}}{G_{mm}}\right) * 100\%$$

where,

AV = Air Void Content [%]

G_{mb} = Bulk Specific Gravity of Compacted Specimen (mass/bulk volume)

G_{mm} = Maximum Specific Gravity of Mixture

After production of the specimen is complete, the bulk specific gravity of the specimen should be determined. Two techniques are typically used to determine the bulk specific gravity of a specimen: The Saturated Surface Dry (SSD) method and the Corelok method. Both methods determine the volume of the specimen by determining the weight of water displaced by the bulk volume of the specimen at 25°C. Since the weight of water at 25°C is equal to 1 gram per cubic centimeter, the weight of water displaced is equal to the bulk volume of the submerged specimen in cubic centimeters. Using the SSD method, the volume of the specimen is found by determining the difference between the weight of the submerged specimen and the weight of the saturated specimen with the surface quickly dried to remove water attached to the specimen via surface tension. This difference is the weight of water displaced by the specimen and thus the bulk volume. The Corelok method determines the volume by vacuum sealing the specimen in a bag with a known volume. The weight of water displaced is the volume of water displaced by the bulk volume of the specimen plus the volume of the bag.

Due to the unique geometry of this test specimen, the author deemed it prudent to determine the bulk specific gravity using both techniques to verify the results. This was because the ratio of surface area to total volume of the proposed specimen layout is significantly higher than that of the compacted cylinders, thus the amount of surface drying in the SSD method has a significantly more pronounce effect on the determined value. A comparison of the results of the two methods for nine consecutive specimens used in this study is summarized in Table 2. As can be seen, the two measurement methods result in similar values, with the average difference being less than 0.01 for this set. To reduce any bias that may be present in either of the methods, the average of the two results was used to determine the air void content of the specimens

throughout the course of this study. It is important to note that such a small difference may be due in part to the very low air voids of these samples.

Table 2: Bulk Specific Gravity Measurement Method Comparison

Specimen I.D.	Gmb (SSD)	Gmb (Corelok)	|Difference|
KMT021	2.375	2.364	0.012
KMT022	2.338	2.338	0.001
KMT023	2.370	2.404	0.034
KMT024	2.418	2.410	0.008
KMT025	2.467	2.466	0.001
KMT026	2.402	2.402	0.000
KMT027	2.405	2.405	0.000
KMT028	2.461	2.444	0.018
KMT029	2.426	2.413	0.013

At North Carolina State University, a study was performed to determine the appropriate size cylindrical specimen for uniaxial fatigue testing (Chehab et al., 2000). During the course of the study, it was found that the air void content of a gyratory compacted cylinder varies significantly over the depth and diameter of the cylinder. Specifically, it was found that, for 150-mm diameter by 115-mm long compacted cylinders, the air void content of the middle 20% by volume (75-mm diameter by 72-mm length) is approximately 2.5% less than the air void content of the full-size cylinder. Based on these findings, a relationship between the air void content of the proposed specimen geometry and the overall air void content of the compacted cylinder should be determined.

The first 21 specimens created during this study were 25-mm thick. This allowed for the production of 3 specimens from every compacted cylinder. The cylinders were all compacted in one lift using the Superpave gyratory compactor per AASHTO Standard T312. A comparison of the air void content of these specimens to the overall air void content is provided in Table 3. The

results indicate that, when producing three specimens from a single cylinder, the air void content of those specimens will be 2-4% less than the overall cylinder air void content.

Table 3: Air Void Comparison for 3 Specimens per Cylinder

Cylinder I.D.	Cylinder AV%	Specimen I.D.	Specimen AV%	Difference	Average Difference
1	3.1%	KMT009	0.4%	2.7%	2.1%
		KMT010	1.1%	2.0%	
		KMT011	1.6%	1.5%	
2	5.5%	KMT012	0.7%	4.7%	3.5%
		KMT013	3.9%	1.6%	
		KMT014	1.3%	4.1%	
3	7.1%	KMT015	1.7%	5.4%	3.9%
		KMT016	5.6%	1.4%	
		KMT017	2.2%	4.8%	
4	6.3%	KMT018	3.7%	2.6%	2.0%
		KMT019	3.2%	3.1%	
		KMT020	6.1%	0.2%	
5	7.9%	KMT021	5.4%	2.5%	2.3%
		KMT022	6.7%	1.2%	
		KMT023	4.7%	3.1%	
6	4.1%	KMT024	1.8%	2.3%	2.8%
		KMT025	-0.3*%	4.4%	
		KMT026	2.3%	1.8%	
7	3.5%	KMT027	2.2%	1.3%	2.1%
		KMT028	0.3%	3.2%	
		KMT029	1.6%	1.9%	

*This negative value is due to slight errors in the specific gravity tests.

One observation worth noting from Table 3 is the significant variability of the air void content from specimen to specimen from a single cylinder. Clearly, even after trimming the outer 10-mm of the cylinder, the air void content varies significantly over the depth of the cylinder. For this reason, it was decided to produce two specimens from each cylinder. This allows for the specimens to be symmetric about mid-depth and thus yield specimens with consistent air void content. A more refined investigation of the air void content of specimens versus the overall

cylinder was performed following this procedure. Three cylinders of the same mix were compacted to 10.2%, 7.1% and 3.7% air void content. Two specimens were produced from each cylinder. The air void content of each specimen was taken at its final geometry as well as at the intermediate stage of discs. This intermediate stage allows for an understanding of how much the air void content decreases with depth while the air void content of the final geometry provides understanding of how the air content decreases radially. A summary of the investigation is included in Table 4. The average air void content difference between the specimens and their respective cylinders was 3.2% less. This is consistent with the previous seven cylinders, however the variability from specimen to specimen is significantly less, suggesting a more predictable air void content when producing only two specimens from a single cylinder. It is also evident that the air void content decreases both with depth and radially, since the air void content of the discs was consistently lower than the full cylinder and higher than the final specimen.

Table 4: Summary of Air Void Content Investigation

Cylinder	**TLO6**		**TLO7**		**TLO8**	
Maximum Specific Gravity	2.439		2.439		2.439	
Overall Cylinder Gmb	2.190		2.267		2.349	
Overall Cylinder AV%	10.2%		7.1%		3.7%	
I.D.	**40**	**41**	**42**	**43**	**44**	**45**
Disc Gmb	2.240	2.256	2.318	2.312	2.388	2.359
Disc AV%	8.2%	7.5%	5.0%	5.2%	2.1%	3.3%
Specimen Gmb	2.264	2.260	2.342	2.358	2.423	2.431
Specimen AV%	7.2%	7.3%	4.0%	3.3%	0.7%	0.3%
Disc Difference	2.0%	2.7%	2.1%	1.9%	1.6%	0.4%
Specimen Difference	3.0%	2.9%	3.1%	3.7%	3.0%	3.3%
Average Specimen Difference	**3.2%**					

4.4 Discussion and Recommendations

The proposed test specimen geometry accomplishes the original objectives of the study. The tapered edge effectively reduces the cross-sectional area to facilitate mid-specimen failure. The geometry of the specimen is such that multiple specimens can be produced from a single gyratory compacted cylinder. The specimens are produced from discs that have been cut horizontally from a cylinder. This orientation allows for specimens to be cut from sample cylinders cored from the field in the same manner.

An additional advantage of this orientation is that the loading axis of the final test specimen orientation is the radial axis of the specimen prior to cutting it from the cylinder. This is advantageous for field samples because the radial axis is the direction in which tensile strains are developed near the bottom due to flexure. In other words, the tensile loading during the test is oriented in the same direction as the tensile strains experienced in the field.

Finally, the fabrication of these test specimens is compatible with standard SPT procedures. The specimens are cut from gyratory compacted cylinders, meaning no split molds or otherwise non-standard compacting equipment is necessary. Coring is not needed for producing these specimens, bypassing one of the production steps required in SPT cylinder production. By adding an intermediate material between the specimen and the steel loading platens, the specimen geometry is also compatible with standard AMPTs.

Producing these specimens involves multiple cutting procedures that are atypical from standard test methods. Slicing the cylinder into discs is relatively simple and similar to the standard procedure of cutting the ends from cored SPT cylinders. The discs then need to be cut into rectangular specimens. This is not a standard procedure; however, it is a very simple process.

The dimensions of the rectangle are marked on the face of the discs, and the cut is made in one pass. The back support of the cutting platform enforces perpendicular cuts, so the operator simply needs to ensure the cut is being made in the correct location. The most involved cutting procedure is the final one. Using a trimming jig, the sides of the specimens are continuously tapered in the form of an arc. This cutting procedure requires attention to detail while setting up the cutting platforms and trimming jig, and the trimming procedure requires patience and attentiveness to safely and accurately perform the cut. Nevertheless, the process is still relatively simple.

There is obvious potential to expedite this production process. In general, the more tools that can be created to facilitate the cutting procedure and reduce the amount of operator effort, the more precise and efficient the procedure will become. Two improvements in particular would drastically improve the process. The first is the use of a saw with a 400-mm diameter blade. This size blade would allow for 150-mm diameter cylinders to be sliced in a single pass which would decrease the required cutting time and improve the quality of the cut. A larger blade will also improve the quality of the trimming. As mentioned previously, the curvature of the blade causes the depth of the cut to vary slightly over the depth (thickness) of the specimen. A larger diameter blade will decrease this curvature. The other potential improvement is a cutting platform with two additional degrees of freedom: an adjustable height and slight rotation about the longitudinal axis. The former would allow for the specimen to be raised to the point tangent with the blade as is necessary in the trimming procedure, without the need for additional platforms. The latter would allow the platform to be rotated slightly to account for warping of the blade over time.

Despite these added cutting procedures, the production of the proposed specimens is comparable to the production of standard SPT test specimens. If multiple cylinders are available for cutting, approximately 6-9 specimens can be produced in 4 hours or less. The modifications satisfy the initial objective of creating a test specimen with a tapered cross-section that is compatible with current testing procedures while simultaneously allowing for the testing of field samples. The following chapter discusses the testing of the specimens and the results of the tests.

CHAPTER 5: TEST RESULTS AND ANALYSIS

The previous chapter described the conceptualization and subsequent development of the proposed test specimen geometry. The next step is to develop a method for testing the specimens in a cyclic fatigue test. The objective in this portion of the study is to determine how the test specimens can be tested using the AMPT hardware and how to interpret the results.

5.1 Test Mixtures

Four asphalt mixtures were used in this study. The gradation of each mix is included in Appendix A. Two of the mixtures are standard Hawaii Department of Transportation used primarily as a highway surface course mix: STIV and STIV-R. They are essentially the same gradation. The difference is the latter mix includes 20% reclaimed asphalt pavement (RAP) by weight. Both mixtures are dense graded, 12.5-mm nominal maximum aggregate size (NMAS) with use a PG 64-16 binder. The STIV mix design uses 6.2% binder content while the STIV-R uses 6.0% binder content, 1.06% coming from the binder included in the RAP material. The STIV and STIV-R mixtures used in this study come from samples collected in the field provided by Grace Pacific, LLC.

The next mixture used in the study was a mix used for construction of an airport taxi lane in Hawaii and identified as FAA3Q. The mix is dense graded with a 12.5-mm NMAS and uses a PG70-22 SBS-modified binder at 5.8% asphalt content. This mixture was also provided from the field by Grace Pacific, LLC.

The fourth and final asphalt mixture used is a thin lift overlay mixture currently being tested by Archilla at the University of Hawaii. The mix is a 9.5-mm NMAS dense graded mixture with a

SBS-modified, PG72-22 binder at 7.5% asphalt content. This mixture was mixed in the lab for this study and identified as TLO.

5.2 Test Method

5.2.1 Specimen Preparation

After the specimens have been cut and all applicable measurements recorded, they should be aged in accordance with AASHTO Standard R30, as is standard for mechanical testing of asphalt mixtures. This involves placing the specimens in a forced draft oven at 85°C for 5 days. The intent is to oxidize the binder sufficiently to mimic the effect of long-term aging experienced by pavements in the field. Next, the specimens must be attached to the loading platens. This involves bonding the phenolic linen pieces to the steel loading platens and subsequently bonding the specimen to the phenolic linen interfaces. The bonding agent used is a plastic steel putty, Devcon 10110. Once the putty has cured, the specimen is ready for testing. The following sections describe this process in further detail.

5.2.1.1 Gauge Point Installation

During testing, the deformation experienced by the specimen is measured by linear vertical displacement transducer (LVDT) strain gauges. The LVDTs must be attached to the specimen. This is done by attaching hexagonal steel gauge points to the sides of the specimen. These gauge points support the clamps which support the LVDTs. In order to transform the raw displacement information recorded during the test to strains, the distance between these gauge points must be known exactly. It is thus critical to use mounting hardware that consistently attach the gauge points at a set distance from each other.

To achieve this, a metal jig is used to hold the gage points at a fixed distance while the gauge points are glued to the specimen. The jig is attached to an acrylic plate which fixes the vertical and horizontal alignment of the gauge points. Finally, a vice is used to apply gentle pressure to ensure the points do not move and facilitate a good bond during the curing process. The bonding agent used has a strength of at least 2500 psi and a full cure time of 1 hour or less. Gorilla Epoxy proved to work well. Figure 19 demonstrates this process.

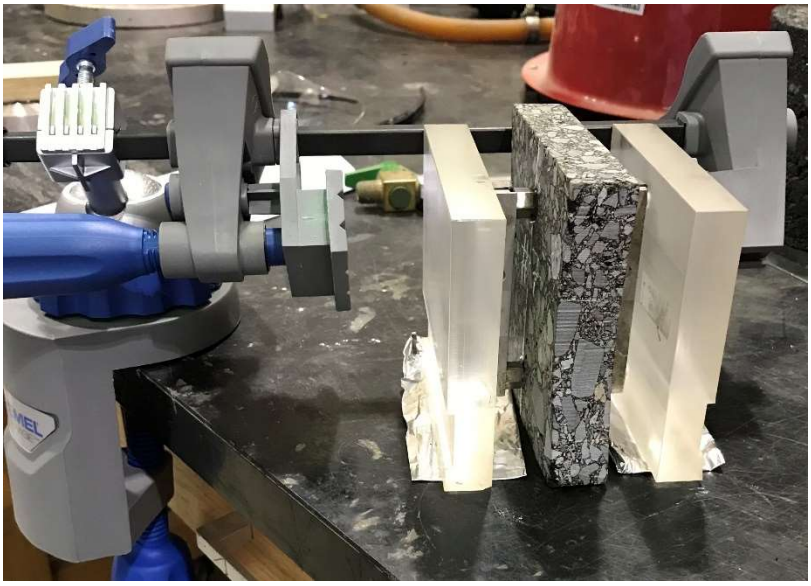

Figure 19: Gauge Point Installation

5.2.1.2 Bonding the Interfaces

Once the gage points have been glued, the specimen is ready to be attached to the loading platens. The bonding agent used is a plastic steel putty, Devcon 10110. Recall from section *4.1.3 Intermediate Material* that an intermediate, phenolic linen block is added between the steel loading platens and the specimen. The purpose of this is two-fold. The first is to provide a plate-to-plate length of approximately 150-mm as is needed for compatibility with the AMPT. The second is the relative stiffness of the materials. Steel is significantly stiffer than asphalt at 40°C

and as such, the bonded interface causes strain concentrations due to differential lateral stresses. Providing an intermediate phenolic linen interface reduces this effect.

The blocks used in this study are 105-mm long by 45-mm wide by 16.33-mm thick. The blocks are centered placing tape on the platen to mark the boundary. The specimen thickness (25-mm or 38-mm) is less than the width of the blocks, therefore the specimen must also be centered within the blocks. It is recommended that the blocks be glued to the platens first and allowed time to cure, prior to gluing the specimen ends to the blocks. While this adds a few hours for the initial bond to set, it was found that having four faces with fresh putty was difficult to prevent from shifting while setting.

Perhaps the most critical aspect in the preparation phase is ensuring concentric alignment and parallel faces during bonding. Any eccentricity will result in a non-uniform stress distribution, distorting the resulting strains. Moreover, a significant eccentricity will cause a couple in the putty interfaces. The weakest bond developed by the putty is to the steel platen. As such, the couple developed between the steel platen and the linen block results in a ripping effect that will cause the bond to fail and thus a failed test. An example of such eccentricity is shown in Figure 20. Needless to say, this test failed as the linen became disconnected from the steel plate after just a few cycles of loading.

Figure 20: Example of an Eccentric Alignment

As previously mentioned, SPT tests are performed on cylinders with a diameter of 100-mm and length of 150-mm. For SPT tests involving tension, such as AASHTO Provisional Standard TP-107, these cylinders must be glued to the steel loading platens. As such, most AMPT machines have a complementary gluing jig to ensure proper alignment while gluing. Such a gluing jig was used for aligning the newly proposed specimens during gluing. The gluing jig used during this study is the IPC Global's Tension Platen Fixing Jig. The jig holds the top platen by magnetic force and holds the lower plate in a grooved opening. This ensures the top and bottom plate remain parallel. For gluing the SPT cylinders to the platens, a clamp is built into the jig to hold the cylinder centered on the plates. Unfortunately, this clamp is not compatible with the newly proposed geometry. Due to the slenderness of the proposed specimen relative to the surface area of the steel platens, the ability to hold the specimen in place is even more critical. To compensate

for this, an adjustable vice is used to hold the specimen in position. This is illustrated in Figure 21.

Figure 21: Steel Platen Gluing Jig

Figure 21 also illustrates the use of aluminum braces. These braces are made from a simple all-thread with adjustable aluminum caps. They are used during the gluing process to ensure the top plate does not rotate slightly about the axis defined by the specimen. They are also used to limit the spread of the putty. The gluing jig was created for the full-size cylinders; therefore, the weight of the top jig was set such that appropriate pressure would be applied during curing. However, this weight was found to be too much for purposes of gluing the proposed specimens, causing the putty to evacuate out of the interface and result in too thin of a bond thickness. The braces are used to control the bond thickness. For example, if the plate-to-plate distance with the specimen in place prior to gluing is 145-mm, the braces are set to a height of 147-mm to ensure a

1-mm thick layer of glue at each interface. Once the gluing procedure is completed, the specimen remains undisturbed for 24-hours to allow the steel putty to completely cure.

5.2.1.3 Installing the Specimen in the AMPT

Once the cure is complete, the specimen is loaded into the AMPT. The AMPT used in this study was an IPC Global's Simple Performance Tester. The aluminum braces discussed in the previous section are left in place for the entirety of the installation process. This ensures that any compressive impact loads exerted by the loading ram during installation can be absorbed by the braces, rather than the specimen.

The first step in the installation process is bolting the lower plate to the actuator. Once the bottom plate is fixed, the LVDTs are mounted onto the gage points and zeroed out. A steel bearing ball is inserted into a groove in the center of the top plate. An equivalent groove is located in the top plate of the reaction frame. The bearing ball ensures the load transfer is concentric. Finally, three small set screws are placed at about 120° above the top load platen. For reasons explained later, these set screws are used to hold fixed the relative angle between the top loading platen and the top plate of the reaction frame.

Once all the hardware is inserted into the load cell, the confining cell is lowered and set to the test temperature. The specimen and the rest of the testing hardware are left undisturbed in the cell until all elements have reached the test temperature. As mentioned in previous sections, this study performed tests at 40°C to better represent the fatigue behavior of pavement at higher temperatures as is applicable to roads in Hawaii at peak traffic demands in the summer months. This is about 20°C higher than the ambient temperature of the lab where these tests were performed. The 38-mm specimens take approximately 5 hours of conditioning time to reach this

temperature. A good indication that the specimen temperature has stabilized is by monitoring the LVDTs. The specimen will stretch at a rate of about 0.0005 mm/second during the initial conditioning. This rate will continue to decrease until the specimen eventually reaches equilibrium. This indicates the specimen has reached the testing temperature.

Next, the aluminum braces are extended to just make contact with the top plate (the braces will not expand as much as the specimen). Then, then actuator ram (connected to the lower platen), is raised slowly until contact is just made between the bearing ball and the top plate of the reaction frame. This will be indicated by a sharp spike in load level (albeit small) which is displayed on the monitor of the computer connected to the AMPT. Note that at this point, a small load (approximately 0.1 kN) is transmitted through the steel ball to the top platen. It is important to stress here the importance of keeping the aluminum braces in place and in contact with the top and bottom platens so that the load is transmitted through the braces and little or no stress is applied to the sample before testing. At this point, unless the gluing process resulted in the top and bottom platens being perfectly parallel (not a realistic result), there will be a slight relative angle between the top platen and the top plate of the reaction frame (i.e., there will be slight lack of parallelism between their faces). If this relative angle is not maintained when bolting the top platen, even without a steel ball, the tightening of the bolts would force the top platen to become parallel to the top plate of the reaction frame which, in turn, would stretch one side of the specimen more than the other. This uneven displacement would cause a non-uniform stress distribution which may affect the results or even force one of the bonded interfaces to fail. However, the test setup described earlier includes the steel ball so that most of the axial load is transmitted through it. In this case, careless tightening of the bolts without the set screws can

result in even larger uneven stretching. Therefore, to maintain the original relative angle, the set screws are placed around the circumference of the top loading platen at 120°. The screws are then extended to just make contact with the top plate of the reaction frame

After the set screws are properly adjusted, the top plates are bolted together. The bolts should be tightened in an alternating fashion to avoid stretching one side of the specimen more than the other (note that the presence of the set screws should limit this differential stretching to a large extent). While tightening the bolts, the actuator should be switched to load-control at a near-zero load. This will ensure the tightening of top bolts does not result in stretching of the specimen.

Once all of the bolts have been tightened, the LVDTs should be re-zeroed and the braces removed so that the loading during the test is applied to the sample. The confining cell can then be lowered, and the specimen is ready for testing. Figure 22 shows an example of a fully installed specimen within the testing chamber.

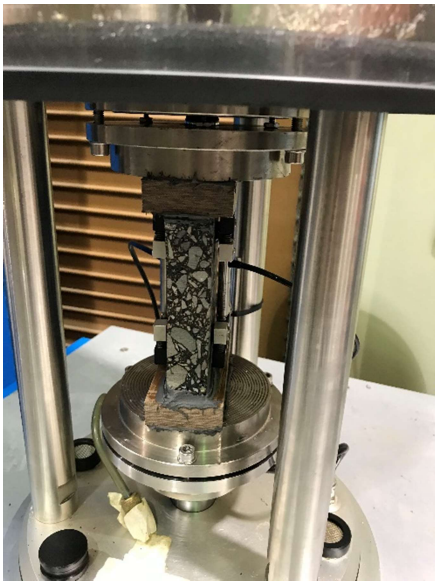

Figure 22: Installing the Specimen into the Testing Cell

5.2.2 Test Parameters

The objective of this study was to develop a new specimen geometry for use in uniaxial fatigue testing. The fatigue testing used in this conceptual study was a crosshead displacement-controlled, cyclic fatigue test. Crosshead displacement-controlled means uniaxial loading is applied in a cyclic manner to induce a constant actuator displacement amplitude each cycle. While an ideal strain-controlled test results in constant *on-specimen* strain amplitude each cycle, achieving this in practice is difficult. A more practical version of the strain-controlled test is to hold the displacement amplitude of the actuator constant. This type of test is known as a constant crosshead cyclic test. This is the type of test used during the course of this study.

The testing software used is the user-programable version of IPC Global's Universal Testing Software: UTS No. 19. This software allows the operator to define the loading and environmental parameters controlled by the AMPT. For a constant crosshead cyclic test, the required testing parameters are relatively straight-forward. The test temperature is held constant at 40°C. The cyclic frequency is set to 10 Hz as is typical for uniaxial fatigue tests. The remaining parameter is the displacement amplitude to be achieved by the actuator each cycle. This is provided by specifying the maximum and minimum absolute displacement as well as the loading pattern the actuator should follow. For this study, a haversine loading pattern was selected.

In a constant crosshead test, the actuator displacement amplitude is not equivalent to the displacement amplitude of the LVDTs since the deformation of all elements within the load path are displacing to some degree. In fact, since fatigue testing results in loss of the material's stiffness, the deformation occurring between the gauge points increases throughout the duration

of the test. This is demonstrated in Figure 23 which plots the strain amplitude of a specimen throughout the duration of a test. The initial strain amplitude exhibited by the specimen will depend on the stiffness of the mixture. As discussed previously in section *3.2 Fatigue Failure Criteria*, a common method of characterizing fatigue behavior of an asphalt mixture in cyclic fatigue testing is determining the relationship between initial strain and number of cycles to failure. Therefore, it is important to be able to roughly estimate the initial strain amplitude based on the specified actuator displacement amplitude. Based on experience, it was determined that the initial cycle-to-cycle deformation amplitude observed within the 70-mm gauge length for the proposed test configuration is approximately half the actuator displacement amplitude. With this rule of thumb, an initial strain is targeted by specifying an actuator displacement amplitude twice the displacement required between the gauge points to result in that strain magnitude. For example, if an initial strain amplitude of 300×10^{-6} is desired, the displacement required within the 70-mm gauge length would be 0.02-mm. To achieve this, an actuator displacement amplitude of 0.04-mm should be specified.

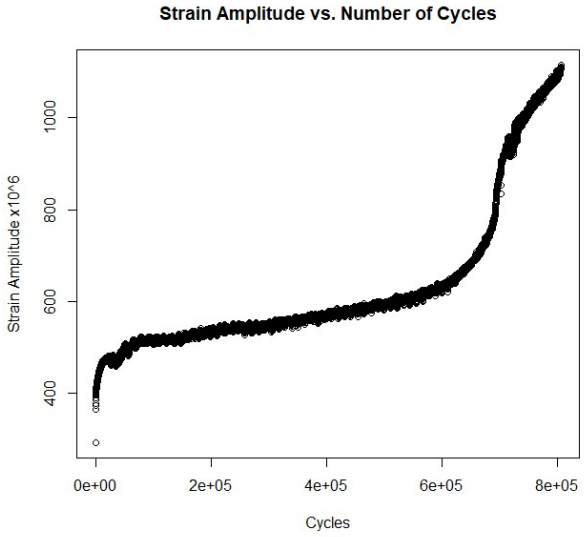

Figure 23: Example of Specimen Strain Amplitude Increasing Throughout Test

5.3 Data Analysis

The intent of an asphalt fatigue test is to observe the behavior of a specimen under repetitive loading. Fatigue damage is assumed to be a result of *tensile* strains. As such, uniaxial fatigue tests are typically performed by inducing repetitive tensile strains. In a constant crosshead cyclic test such as the one used in this study, these tensile strains are developed by cyclically pulling the actuator from its initial location – at which point no stress is being applied to the specimen - to a specified displacement amplitude and then back to its initial position. Figure 26 demonstrates the actuator movement achieved during the test. The LVDT displacement, shown in Figures 23 and 24, shows that the specimen is being stretched from its initial position with a continually increasing amplitude. This increase in amplitude is due to the damaging of the material.

For a purely elastic material, the reverse motion back to the initial position by the actuator would be accomplished simply by unloading the specimen at an equal and opposite rate to that used to achieve the initial displacement amplitude. Due to the viscoelastic nature of asphalt, however, in

order to reverse the actuator back to its initial position in the same amount of time used to displace it, a compressive force is required. Figure 27 plots the force measured by the actuator over the course of 10 cycles at a random point in a test. The plot shows that an equal amount of compressive and tensile energy is required to achieve the specified displacements even though the actuator never moves in a 'pushing' direction relative to its initial location. In short, the viscoelasticity of the asphalt concrete causes the stress-strain relationship to be time dependent. Since fatigue is characterized by a loss in stiffness, this time-dependency complicates the analysis. This is why the development of viscoelastic continuum damage theory in asphalt concrete fatigue is so attractive. The theory separates the elastic and viscoelastic effects via a correspondence principle so that the change in stiffness due to viscous effects is isolated from the change in stiffness due to damage. This concept is described in more detail in section 3.1.3 Direct Tension Fatigue Tests.

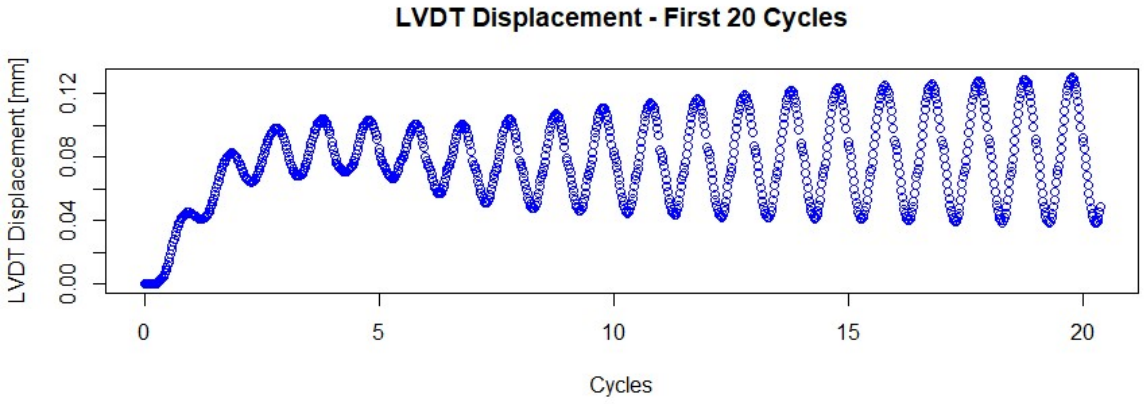

Figure 24: LVDT Displacement Readings - First 20 Cycles

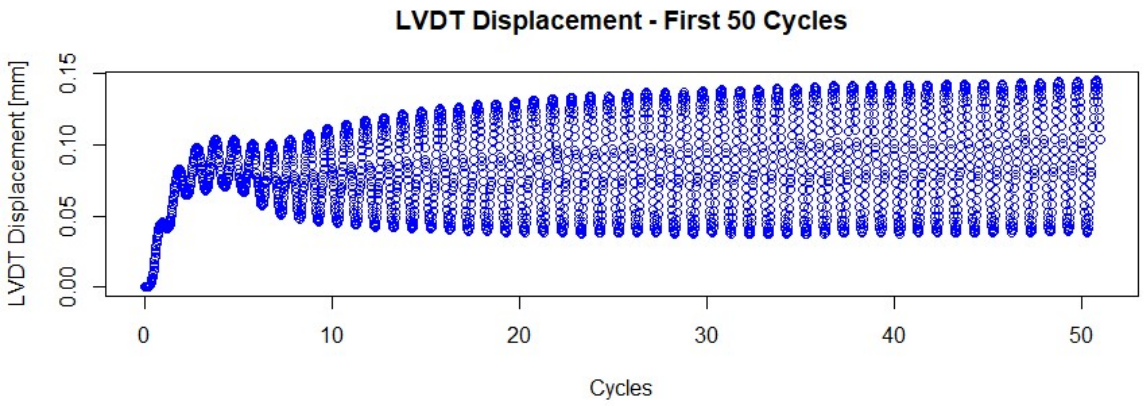

Figure 25: LVDT Displacement Readings - First 50 Cycles

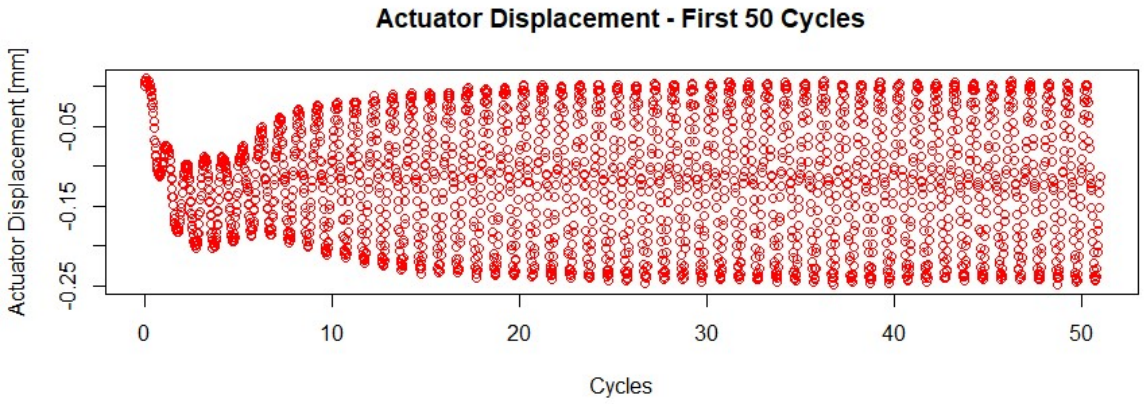

Figure 26: Actuator Displacement Readings - First 50 Cycles

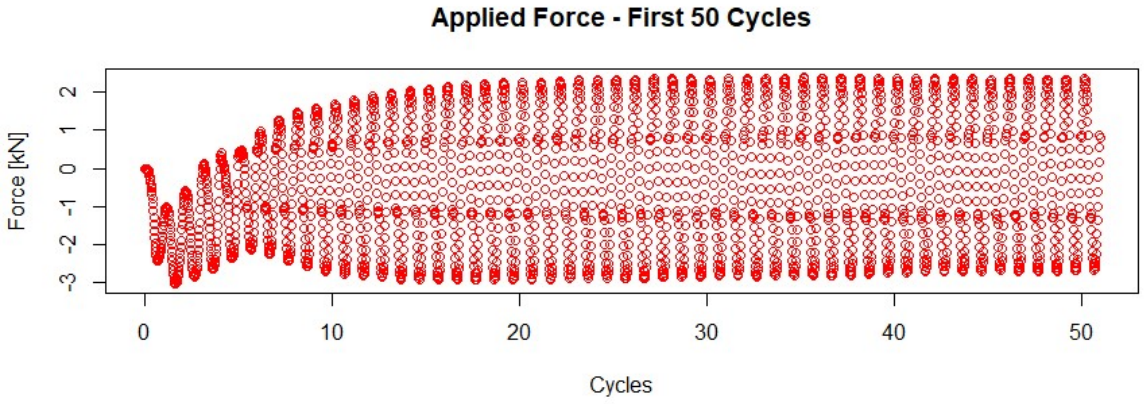

Figure 27: Applied Force Readings - First 50 Cycles

The intent of this study was to develop a new specimen geometry and determine whether uniaxial, cyclic fatigue testing could be performed using these specimens. For simplicity, the analysis of the fatigue tests was limited to determining the amplitudes for the stress at the center of the specimen and the strain measured by the two LVDTs for each cycle. The stiffness of the mixture is then determined at each cycle based on these values. For the purposes of this study, stiffness was taken simply as the ratio of the stress amplitude at the middle of the specimen to the average strain amplitude.

The raw data recorded by the transducers throughout the test typically has some noise associated with the signal. As such, post-processing calculated values, such as stiffness, are difficult to determine accurately from the raw data alone. In order to use reasonable values in the analysis, a sine wave is fit to the raw data for the stress as measured by the actuator and for the strains as measured by each LVDT. The fitting procedure used a simple linear regression similar to that described in AASHTO Standard T342-11 for determining dynamic modulus via uniaxial cyclic loading (AASHTO, 2016). The regression was performed in the software environment, R. The complete script is available in APPENDIX B: DATA ANALYSIS SCRIPT. An illustration of the fitting procedure is provided in Figure 28.

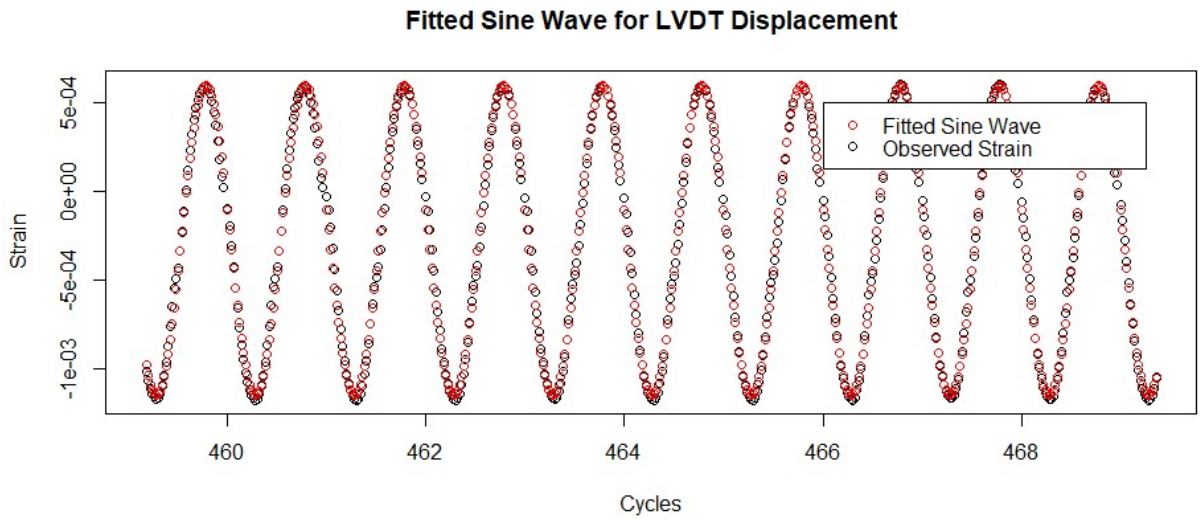

Figure 28: Comparison of Raw Strain to Fitted Sine Wave

The fatigue behavior of a specimen was characterized by observing the reduction in stiffness over the course of the test. An example of this behavior is shown in Figure 29. This stiffness reduction plot can be used to determine the point of failure for that test. The number of cycles to failure is then used as means of comparison between different mixtures tested under similar loading and environmental conditions or between specimens from the same mixture with variable loading or environmental conditions.

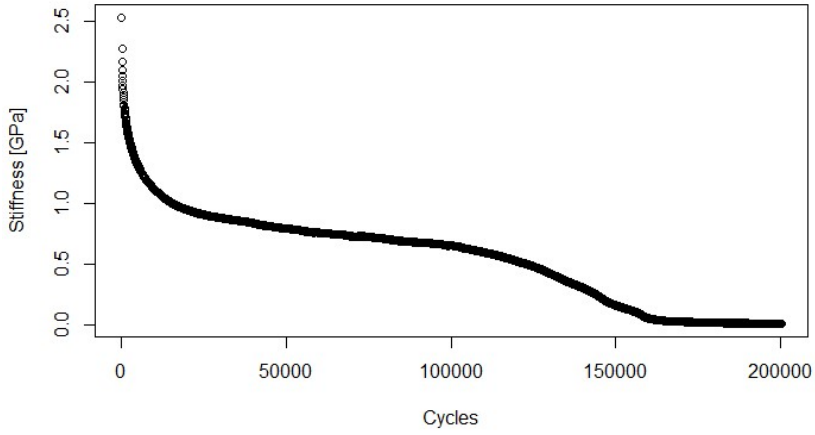

Figure 29: Stiffness Reduction of a Specimen During a Fatigue Test

5.4 Failure Criterion

In Chapter 3, the concept of failure criterion for fatigue tests was described in detail. Based on this discussion, a precise definition of failure is needed for accurate data analysis and comparisons. Furthermore, this definition should represent a point at which a fundamental change in material integrity occurs. Many definitions have been established attempting to accomplish that objective. Since the main purpose of this study is a proof of concept, a simplified definition of failure was adopted.

Refer again to Figure 29. There are three primary stages in the stiffness reduction. The first stage involves a rapid decrease in stiffness. This rate of decrease quickly diminishes until an approximately constant rate of change is observed. This constant rate is the second stage. The second stage ends and the final stage begins when this rate of reduction ceases to be constant and begins to increase rapidly. The second stage represents a steady but stable reduction in stiffness. This stable decrease suggests that the integrity of the material is still intact. However, the third stage represents stiffness reduction at an unstable rate. Clearly, the material integrity is deteriorating at a fundamental level. This stage occurs when the microcracks developed throughout the course of the fatigue test coalesce into macrocracks.

The transition from the second to the third stage of stiffness reduction seems to be the critical point at which the specimen transitions from acceptable to unacceptable damage. As such, this study defines failure as the cycle at which the curvature in this transition region is at a maximum absolute value. The previous section described the process of fitting a sine wave to the raw data recorded during the tests. These fitting parameters can be used to determine the stiffness at any given cycle. By plotting the stiffness versus cycles for a given test, the stiffness reduction plot is

created. Using this same data with an appropriately chosen time step (say, 10% of the total number of cycles), the second derivative of the stiffness with respect to cycles can be approximated numerically. The minimum value of the numerically approximated second derivative, i.e., maximum curvature, is defined as the point of failure. This concept is illustrated in Figure 30. The scripts used to perform the analysis are provided in APPENDIX B: DATA ANALYSIS SCRIPTS.

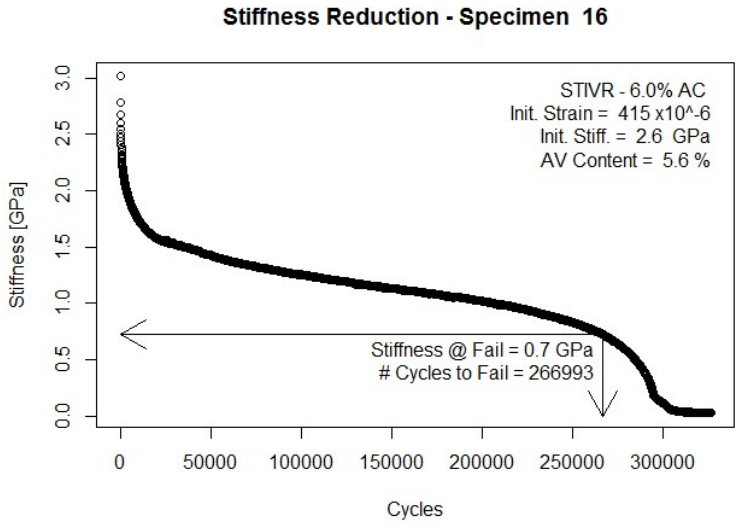

Figure 30: Failure Criteria Based on Stiffness Reduction Plot

5.5 Results

5.5.1 Discussion of Tests Performed To-Date

To date, 37 specimens have been produced. Relevant information for all 37 specimens is provided in APPENDIX C: SPECIMEN INFORMATION. Of these 37 specimens, 32 have been tested in cyclic fatigue tests. The first 6 specimens were tested prior to the use of set screws when bolting the top plates resulting in eccentric loading. After the set screws were added, 5 tests resulted in the linen detaching from the steel platen. These instances were found to be due to

either improper alignment or the improper application of the steel putty. One test ended prematurely due to an error associated with the AMPT. This leaves 20 tests that were run properly according to the procedure laid out in the previous sections. The 20 tests resulted in 19 failures between the gauge points and 1 end failure: a 95% success rate. This information is summarized in Table 5. An example of a successful middle failure is provided in Figure 31.

Figure 32 shows a collection of successful middle failures.

Figure 31: Example of a Successful Middle Failure

Figure 32: Collection of Successful Middle Failures

Table 5: Summary of Tests Performed to Date

Specimen I.D.	Mixture	Result	Comment
KMT001	Unknown	Interface Separation	Set screws not used
KMT002	Unknown	Interface Separation	Set screws not used
KMT003	Unknown	Middle Failure	Set screws not used
KMT004	Unknown	Interface Separation	Set screws not used
KMT005	Unknown	Middle Failure	Set screws not used
KMT006	Unknown	Interface Separation	Set screws not used
KMT007	Unknown	Middle Failure	
KMT008	FAA3Q-1636-14K	Middle Failure	
KMT009	FAA3Q-1636-14K	Middle Failure	
KMT010	FAA3Q-1636-14K	Middle Failure	
KMT011	FAA3Q-1636-14K	Middle Failure	
KMT012	STIV	Middle Failure	
KMT013	STIV	Middle Failure	
KMT014	STIV	Middle Failure	
KMT015	STIVR	Middle Failure	
KMT016	STIVR	Middle Failure	
KMT017	STIVR	Middle Failure	
KMT018	STIV	Interface Separation	Improper Alignment
KMT019	STIV	Middle Failure	
KMT020	STIV	End Failure	
KMT021	STIVR	Interface Separation	Improper Gluing
KMT022	STIVR	Interface Separation	Improper Gluing
KMT023	STIVR	Middle Failure	
KMT024	FAA3Q-1636-14K	Middle Failure	
KMT025	FAA3Q-1636-14K	Middle Failure	
KMT026	FAA3Q-1636-14K	Interface Separation	Improper Alignment
KMT027	FAA3Q-1636-14K	Middle Failure	
KMT028	FAA3Q-1636-14K	Interface Separation	Improper Gluing
KMT029	FAA3Q-1636-14K	Middle Failure	
KMT032	TLO	Not Yet Tested	
KMT033	TLO	Not Yet Tested	
KMT034	TLO	Not Yet Tested	
KMT035	TLO	Not Yet Tested	
KMT036	TLO	AMPT Error	
KMT037	TLO	Not Yet Tested	
KMT038	TLO	Middle Failure	
KMT039	TLO	Middle Failure	

The results indicate that this newly proposed specimen geometry accomplishes the objectives of the study. The tapered cross-section is apparently effective in drastically reducing the expected number of end failures. The test specimens are cut from compacted cylinders in such a way that specimens can be produced from field cores with lifts as thin as 25-mm. Finally, the specimen production and testing can be performed entirely with standard SPT equipment with the one addition of a trimming jig used to taper the longitudinal sides of the specimen.

The major challenge is clearly the proper alignment and application of the putty when bonding the various interfaces. Any eccentricities introduced into the load path during cutting, gluing or installation of the specimen will result in the separation of the platen from the interface and thus a wasted test specimen. For this reason, a slight modification to the gluing procedure is currently being developed. The concept is to use an aluminum loading platen with an acrylic rod bolted to the platen face and permanent, adjustable set screws attached to the ends. The specimens can be glued directly to the rods, bypassing the need to glue the phenolic linen rods to the loading platens. This should significantly reduce the amount of mis-alignment introduced during the gluing process and eliminate the time and expense needed to glue the phenolic linen pieces to the platens. This is illustrated in Figure 33.

Figure 33: Test Specimen Set-Up Using Acrylic Interface

Despite the challenge of properly producing and installing the specimens, the proposed specimen geometry meets the objectives laid out by this study. If the procedures are properly followed, the fatigue tests result in mid-specimen failures and the specimen itself is compatible with both field samples and standard SPT equipment.

5.5.2 Analysis of the Tests

In addition to the high percentage of middle failures, the data generated by the tests appears to be consistent and reasonable. After each test, the raw data recorded is analyzed and the failure point located using the procedure described in the previous two sections. In short, the data generated by a successful test is used to produce a stiffness reduction plot. This plot can be used directly to compare to other tests, or it can be used to find the number of cycles to failure, which is in turn used for comparison.

A stiffness reduction plot was generated for each of the successful tests, and all of these plots are available in APPENDIX D: STIFFNESS REDUCTION PLOTS. The exceptions are for specimens KMT007 and KMT008. Prior to specimen KMT009, the specimen production and testing procedures were still being developed. As such, only a limited amount of data was being recorded by the AMPT for these early tests. In place of the stiffness reduction plots, a plot of the raw actuator load and LVDT displacement amplitudes recorded by the UTS software is provided. As an example, Figure 34 shows the stiffness reduction of three specimens cut from the same overall compacted cylinder. The air void content and initial strain for the three specimens are provided. The similarity of the three plots implies that the test procedure produces consistent results for specimens cut from the same cylinder, even with the variation in air void content.

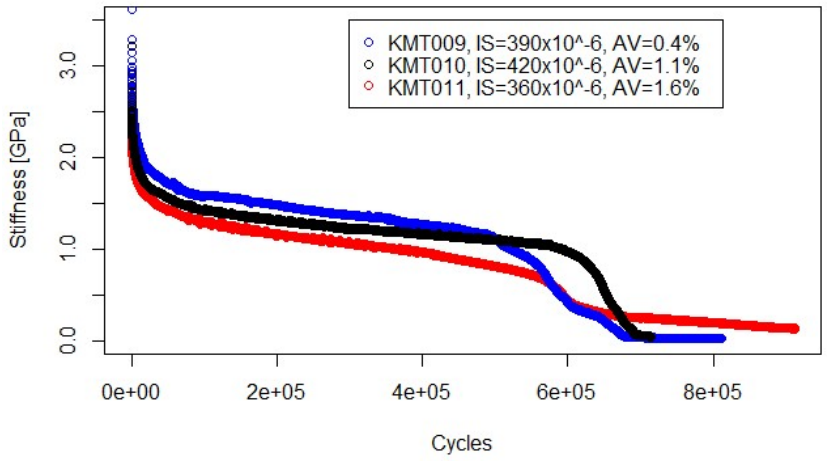

Figure 34: Stiffness Reduction Comparison for Common Mixture

The intent of this study was to develop a new specimen geometry for use in fatigue testing. The high frequency of mid-specimen failures resulting from the tests performed thus far shows that the new specimen geometry accomplishes the intended objectives. The behavior of the specimens during testing, demonstrated by the stiffness reduction plots, is consistent with the

expected behavior of asphalt specimens subjected to constant crosshead cyclic testing. This shows that the testing of these specimens can be used to characterize the fatigue behavior of asphalt mixtures. Unfortunately, the novelty of this specimen fabrication process resulted in highly variable air void content from specimen to specimen. Consistent air void content is critical in accurate comparison of performance test results. As such, further analysis of the performance testing capabilities of this proposed test method with controlled air void content is necessary. Even so, the sheer number of specimens tested during the course of this study allows for some analysis of mixture performance. In particular, two general observations are inferred from the analyses.

The first observation is that this proposed testing method conforms to the traditional fatigue characterization method. As previously discussed, this traditional method assumes a linear relationship between the log of number of cycles to failure vs. the log of the initial strain. This method can be used to compare mixtures by plotting said values and comparing the best fit line associated with the data. This assumed relationship was observed to hold true for the new specimens. Figure 35 demonstrates this analysis. The results from the successful tests are plotted and grouped based on the mixture of the test specimen. The results appear to be reasonable. The FAA3Q, TLO and STIV specimens all demonstrate very similar relationships. The mixes with the modified binder, TLO and FAA3Q, performed better than the mixes with virgin binder. Note that the R^2 value for the TLO mixture is irrelevant since only two data points were available at this time, however the resulting line is logical based on the other relationships.

The obvious exception to this generally encouraging result is the STIV-R mix specimens. The results for these specimens does not fit well to the assumed relationship. The reason for this is

the wide range of air voids. The STIV-R specimens ranged from 2.0-5.5% air void content. Specimens with this large of a difference in air voids are essentially different mixtures all-together, and as such should be ignored in this plot. This is further illustrated in the second observation made based on the results.

The other primary observation made based on the test results is the effect of air voids on fatigue life. It is a well-known concept that increasing the air void content will decrease the fatigue performance of a mixture. This is logical, since air voids essentially reduce the effective cross-section of the specimen. This concept is of particular concern to this study because it was found that the air void content of the proposed specimen geometry varies significantly from the air void content of the compacted cylinders. The test results from these newly proposed specimens reflect this anticipated behavior. Interestingly, the results for the STIV and STIV-R specimens indicate that there is an optimal air void content for fatigue performance, below which the fatigue performance goes down. Figure 36 demonstrates this observation. The plot includes all of the test results from specimens subjected to a 0.08-mm actuator displacement amplitude, since this results in similar initial strains. More tests are needed to confirm this concept.

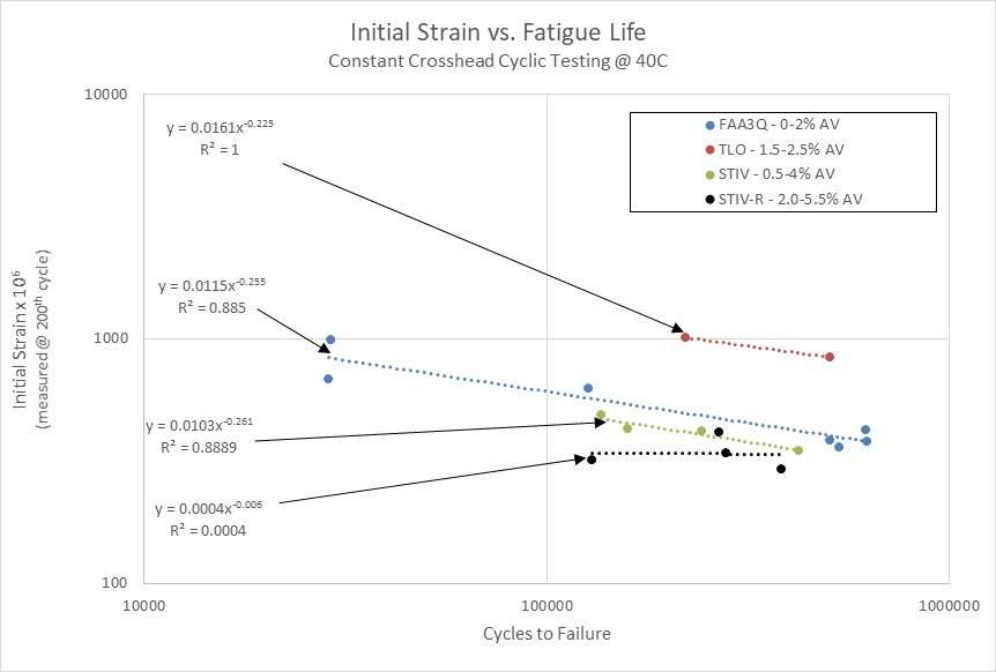

Figure 35: Initial Strain vs. Cycles to Failure

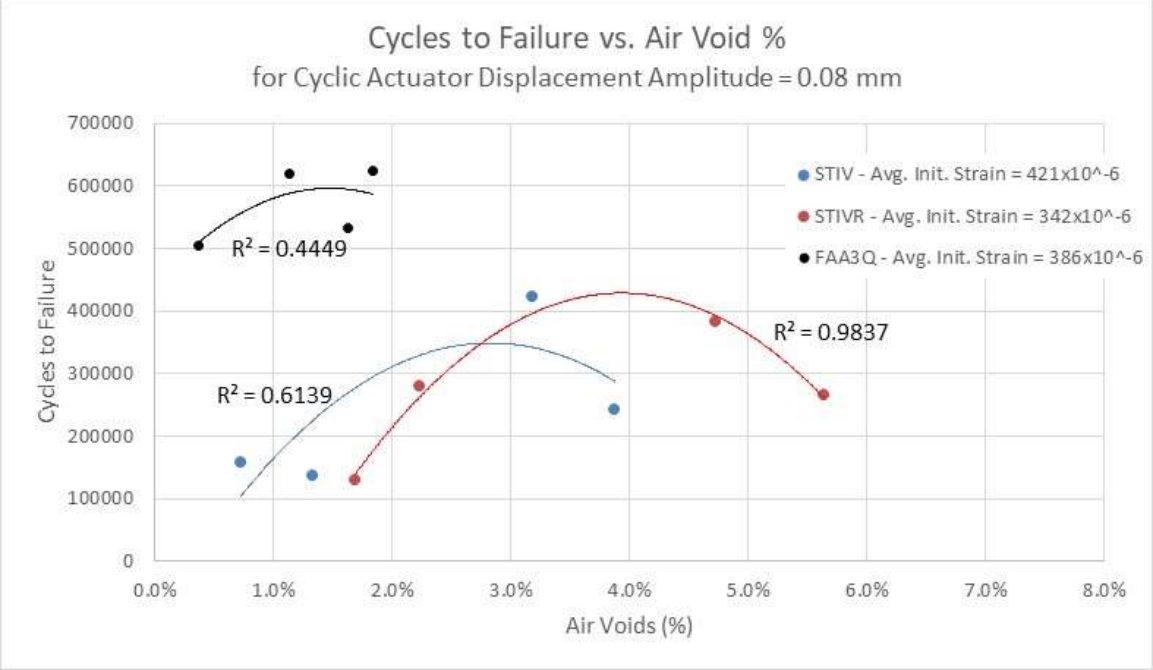

Figure 36: Cycles to Failure vs. Air Void Content

CHAPTER 6: CONCLUSIONS AND FUTURE WORK

6.1 Summary

There is a critical need for an efficient and reliable test method to evaluate the fatigue performance of asphalt concrete. NCHRP Project 9-29 has led to the commercial use of the AMPT for testing the performance of asphalt mixtures. Thus, an efficient fatigue test should be compatible with this testing method. This has led to the creation of the AASHTO Provisional Standard TP-107 as a means of characterizing fatigue performance. However, this test, and other uniaxial fatigue tests utilizing cylindrical specimens, has several challenges associated with it. The tests often result in end failures, or failure regions that develop outside the gauge length of the LVDTs due to strain concentrations that develop at the bonded interface as well as uneven air void distribution. Additionally, the use of 150-mm long test cylinders is also incompatible with most in-situ samples cored from the field because pavements are typically constructed in lift thicknesses of 38 – 150-mm.

The test specimen geometry proposed in this test overcomes these challenges. The proposed specimen is prismatic, 110-mm long, 100-mm wide and the thickness can vary as needed with an ideal thickness of 38-mm. The narrow faces along the 110-mm long sides are continuously tapered at a radius of 175-mm over the middle 90-mm, resulting in an 88-mm width at mid-depth. The tapered cross-section increases the strain within the middle of the specimen sufficiently to overcome the strain concentrations that develop at the ends. The orientation allows for test specimens to be produced from a field-cored sample without the inclusion of multiple lifts. An additional advantage of this orientation is that the test induces tensile strains within the

specimen in the same direction as that induced in the field due to bending (radially with respect to the original cylinder).

Constant crosshead cyclic fatigue tests were performed on a number of these proposed specimens. For the tests that followed the final specified fabrication and testing procedure, 95% of the tests resulted in mid-specimen failures. The results of each test were summarized via a stiffness reduction plot which represents the accumulation of damage throughout the course of the test. Using a simple failure criterion where failure is defined as the point of maximum curvature during the unstable reduction in stiffness, the resulting Initial Strain vs. Cycles to Failure yielded reasonable results. Based on these findings, the proposed test specimen appears to be a potential method for efficiently and reliably testing and comparing the fatigue performance of different asphalt mixtures.

6.2 Future Work

The test specimen fabrication process and test method proposed in this study compares to that of the standard cylindrical fatigue test in terms of required preparation time and effort. The added cutting and bonding time is offset by the advantage of yielding multiple specimens from a single cylinder (not to mention the time saved by avoiding unusable tests due to end failure). With that said, there is significant potential for improving the efficiency of the specimen fabrication process. One such improvement is the use of a customized loading platen to avoid the need for the phenolic linen interface. A prototype is currently being tested for this purpose. An acrylic bar is bolted to an aluminum plate with adjustable set screws embedded in the plate. The stiffness of the aluminum and acrylic are more compatible with asphalt concrete, alleviating the strain concentrations enforced at the ends by the steel plates. This configuration avoids the need for

gluing the phenolic linen to the plates, reducing both the added preparation time and potential for eccentric surfaces associated with the gluing process. This concept is demonstrated in Figure 37.

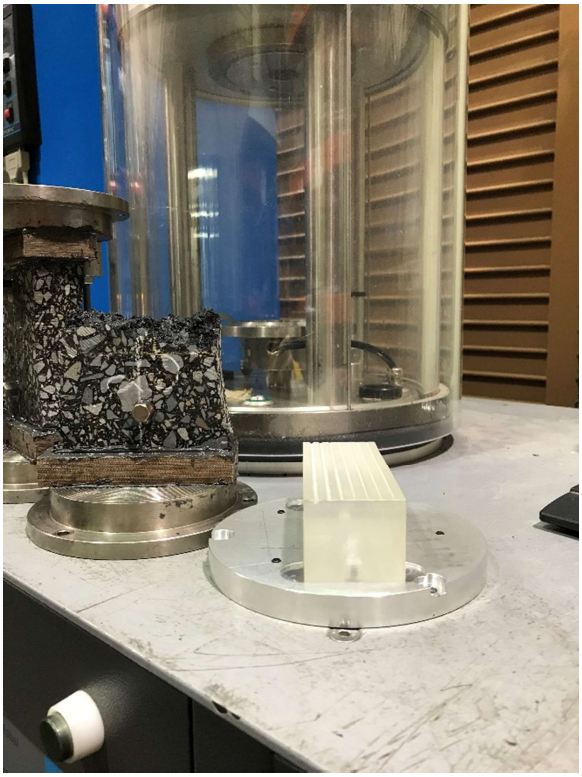

Figure 37: Aluminum Loading Platen with Acrylic Bar Interface

Another potential improvement in the fabrication process is the refinement of the trimming procedure. Recall from section 4.2 Specimen Preparation that there are three phases in the cutting process. The first two, slicing the cylinder into discs and cutting the rectangular specimens from the discs, are relatively simple cuts that can be performed with a typical diamond blade saw used for cutting asphalt concrete. The third phase, trimming the sides of the specimen, requires the use of a customized jig and an atypical cutting procedure wherein the specimen is moved perpendicular to the blade in an arced motion. The cutting procedure is viable after some practice; however, a more refined method would increase efficiency and reduce the variability of the cut from specimen to specimen. One such refinement would be a tongue and

groove mechanism between the jig and the cutting platform to guide the tangential movement of the cut. Ideally, the cutting procedure could be bypassed altogether through the use of a coring machine or similar device to remove the arc in one pass.

In addition to the potential for improved fabrication processes, there is significant potential for further testing of the newly proposed specimens. The method of producing specimens tested during this study evolved as more refined techniques were discovered. This resulted in a wide range of specimen air void content. The air void study revealed that producing two, 38-mm thick specimens from the middle of a gyratory compacted cylinder yields more consistent specimens than producing three, 25-mm thick specimens. It was also found that the former process consistently results in specimen air void content approximately 3% less than the air void content of the overall cylinder. With this in mind, specimens can be produced at a target air void content and fatigue test results compared to better understand the consistency of the results. These test results should also be compared to the test results of standard cylinders with equivalent air void content.

APPENDIX A: ASPHALT MIXTURE GRADATION CURVES

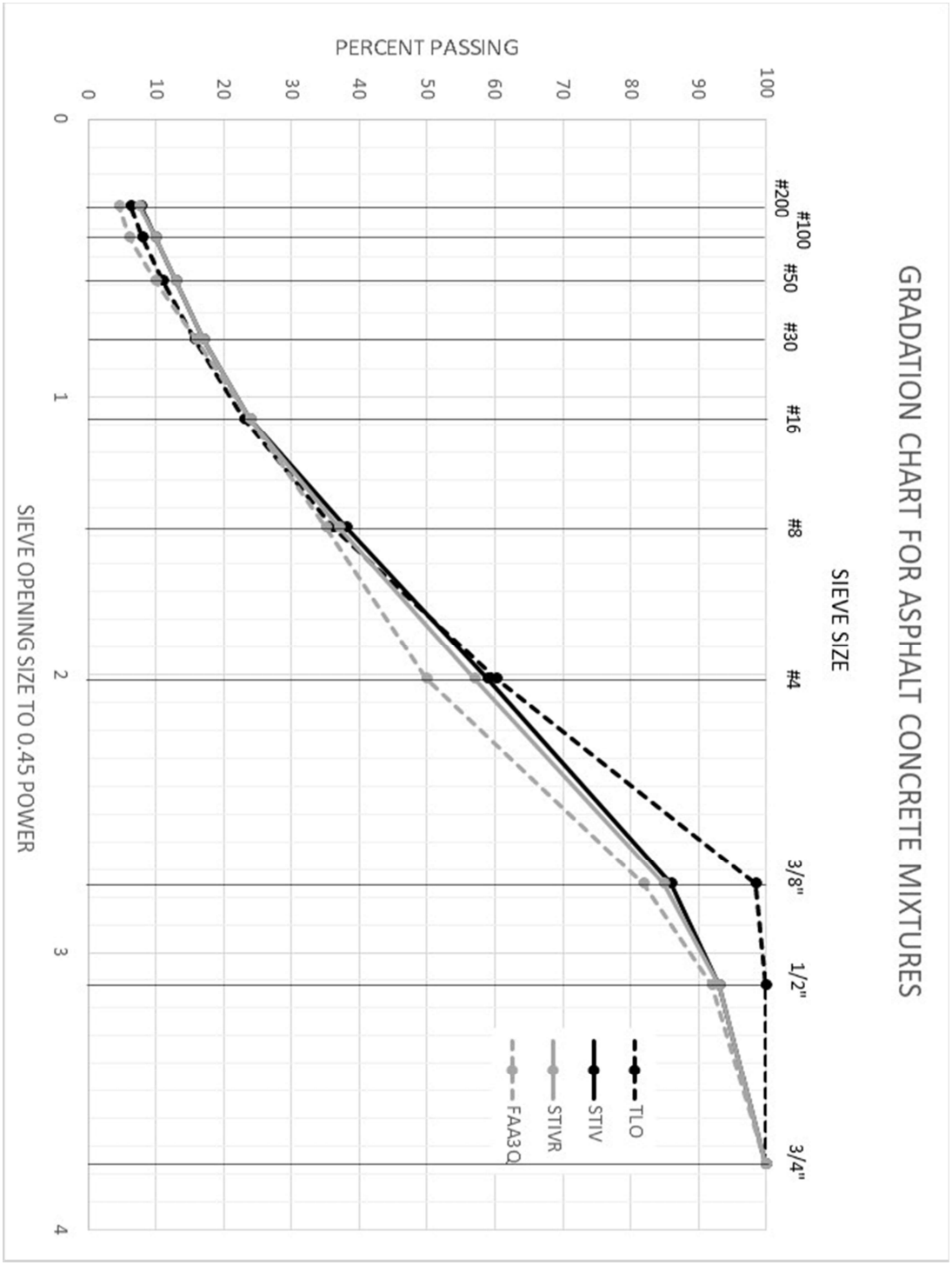

APPENDIX B: DATA ANALYSIS SCRIPTS

This appendix provides the two scripts used in the analysis of the data. The first script reduces the raw data recorded by the transducers through the duration of the fatigue test (.csv format) to a set of vectors summarizing the time, stiffness, phase angle, strain amplitude and stress amplitude for a given interval of cycles. The second script uses this summarized data to develop the stiffness reduction plots and determine the point of failure.

DATA REDUCTION SCRIPT

```
# This script is used to analyze and summarize the raw data recorded
# during a typical fatigue test. The script reads in a 'chunk' of data,
# converts the force and displacements to stress and strain, then fits a
# sine wave to the stress and strain data. The fitted sine wave is then
# used to determine the dynamic modulus and phase angle (following the general procedure
# of AASHTO T342-11) observed over course of the 'chunk' being analyzed.
# The script produces vectors containing the dynamic modulus, phase angle,
# and peak-to-peak stress and strain amplitudes determined for each 'chunk' of data
# A vector containing the median time for each of these chunks is also created

setwd("C:/Users/Grant/Desktop/Thesis/Test Results/KMT013") # file path of the test data
SpecNum<-013 #Specimen identification number
SheetNames<-list.files()
numSheets<-length(SheetNames)
tstep<-.002 #time step of the data recording, specified in the test software
freq<-10 # cyclic frequency in Hz at which the fatigue test is performed
GroupLength<-2500 # number of data points included in a 'chunk'
width<-89 #width of the test specimen at midheight
thickness<-23.7 #thickness of specimen at midheight
area<-width*thickness

#allocate vectors
DynMod<-numeric(0)
PhAng<-numeric(0)
```

```
Time<-numeric(0)
StressMagVec<-numeric(0)
StrainMagVec<-numeric(0)

#determine the initial LVDT values to measure strains from
Sheet1<-read.csv(SheetNames[1],header = TRUE)
initialDisp1<-Sheet1[1,5]
initialDisp2<-Sheet1[1,6]

# loop through each sheet, reading in one sheet at a time
for (i in 1:numSheets){
 curSheet<-read.csv(SheetNames[i],header = TRUE)

 #determine how many complete 'chunks' are included in the sheet
 NumRows<-length(curSheet[,1])
 NumGroups<-floor(NumRows/GroupLength)

 #systematically extract one 'chunk' of data at a time to be analyzed
 for (j in 1:NumGroups){
  curStartRow<-(j-1)*GroupLength+1
  curData<-curSheet[curStartRow:(curStartRow-1+GroupLength),]
  curRawStress<-curData[,3]/area
  curRawStrain1<-(curData[,5]-initialDisp1)/70
  curRawStrain2<-(curData[,6]-initialDisp2)/70
  curTime<-curData[,1]

  #Stress Magnitude and Phase Angle
  curAvgStress<-mean(curRawStress)
  #center stress about the average to imitate a 'true' sine wave
  curCentStress<-curRawStress-curAvgStress
  #perform standard linear regression assuming a sine wave function
  StressReg<-lm(curCentStress~cos(2*pi*freq*curTime)+sin(2*pi*freq*curTime))
  #extract parameters from fitted sine wave to be used in determining amplitude and phase
  Aso<-StressReg$coefficients[1]
  As1<-StressReg$coefficients[2]
  Bs1<-StressReg$coefficients[3]

  # The peak-to-peak strain magnitude is twice the amplitude of the fitted sine wave
  StressMag<-sqrt(As1^2+Bs1^2)*2
  StressPhaseAng<-atan(-Bs1/As1)
```

```
#Determine Strain Drift Rate by estimating a linear change in max and minimum values
numCycles<-GroupLength*tstep*freq
NumRowsinCycle<-1/freq/tstep
MaxStrains1<-numeric(numCycles)
MaxStrainsTime1<-numeric(numCycles)
MinStrains1<-numeric(numCycles)
MinStrainsTime1<-numeric(numCycles)
MaxStrains2<-numeric(numCycles)
MaxStrainsTime2<-numeric(numCycles)
MinStrains2<-numeric(numCycles)
MinStrainsTime2<-numeric(numCycles)

for (k in 1:(numCycles)){
  MaxStrains1[k]<-max(curRawStrain1[((k-1)*NumRowsinCycle+1):(k*NumRowsinCycle)])
  MaxStrainsTime1[k]<-min(curTime[curRawStrain1==MaxStrains1[k]])
  MinStrains1[k]<-min(curRawStrain1[((k-1)*NumRowsinCycle+1):(k*NumRowsinCycle)])
  MinStrainsTime1[k]<-min(curTime[curRawStrain1==MinStrains1[k]])
  MaxStrains2[k]<-max(curRawStrain2[((k-1)*NumRowsinCycle+1):(k*NumRowsinCycle)])
  MaxStrainsTime2[k]<-min(curTime[curRawStrain2==MaxStrains2[k]])
  MinStrains2[k]<-min(curRawStrain2[((k-1)*NumRowsinCycle+1):(k*NumRowsinCycle)])
  MinStrainsTime2[k]<-min(curTime[curRawStrain2==MinStrains2[k]])
}
MaxDrift1Reg<-lm(MaxStrains1~MaxStrainsTime1)
MinDrift1Reg<-lm(MinStrains1~MinStrainsTime1)
D1<-(MaxDrift1Reg$coefficients[2]+MinDrift1Reg$coefficients[2])/2
MaxDrift2Reg<-lm(MaxStrains2~MaxStrainsTime2)
MinDrift2Reg<-lm(MinStrains2~MinStrainsTime2)
D2<-(MaxDrift2Reg$coefficients[2]+MinDrift2Reg$coefficients[2])/2

#Strain Magnitude and Phase Angle
curAvgStrain1<-mean(curRawStrain1)
curAvgStrain2<-mean(curRawStrain2)
#center strain about the average and remove drift effect to imitate a 'true' sine wave
curCentStrain1<-curRawStrain1-D1*curTime-curAvgStrain1
curCentStrain2<-curRawStrain2-D2*curTime-curAvgStrain2
#perform standard linear regression assuming a sine wave function and determine coefficients
StrainReg1<-lm(curCentStrain1~cos(2*pi*freq*curTime)+sin(2*pi*freq*curTime))
Aeo1<-StrainReg1$coefficients[1]
Ae11<-StrainReg1$coefficients[2]
```

```
  Be11<-StrainReg1$coefficients[3]
  StrainReg2<-lm(curCentStrain2~cos(2*pi*freq*curTime)+sin(2*pi*freq*curTime))
  Aeo2<-StrainReg2$coefficients[1]
  Ae12<-StrainReg2$coefficients[2]
  Be12<-StrainReg2$coefficients[3]

  # The peak-to-peak strain magnitude is twice the amplitude of the fitted sine wave
  StrainMag1<-sqrt(Ae11^2+Be11^2)*2
  StrainMag2<-sqrt(Ae12^2+Be12^2)*2
  AvgStrainMag<-(StrainMag1+StrainMag2)/2
  StrainPhaseAng1<-atan(-Be11/Ae11)
  StrainPhaseAng2<-atan(-Be12/Ae12)
  AvgStrainPhaseAng<-(StrainPhaseAng1+StrainPhaseAng2)/2

  #Determine Dynamic Modulus and Phase Angle and append vectors
  curDynMod<-StressMag/AvgStrainMag
  curPhaseAng<-AvgStrainPhaseAng-StressPhaseAng
  StressMagVec<-append(StressMagVec,StressMag)
  StrainMagVec<-append(StrainMagVec,AvgStrainMag)
  DynMod<-append(DynMod,curDynMod)
  PhAng<-append(PhAng,curPhaseAng)
  Time<-append(Time,mean(curTime))
 }
}
```

STIFFNESS REDUCTION PLOT AND FAILURE ANALYSIS

```
#Determine Failure Time at Peak Negative Curvature of Stiffness Curve
library(readr)

#These lines require user input (or validation)
specnum<-13 #Specimen number to be analyzed
AV<-3.9 #specimen air void content
Mix<-"STIV - 6.2% AC" #specimen mixture type and asphalt content
freq<-10 #specify frequency in Hz


fname<-paste("C:/Users/Grant/Desktop/Thesis/Test Results/DF",specnum,sep = "") #file name for relevant data
frame
DF<-read_csv(fname, col_types = cols(X1 = col_skip())) #read specified data frame
D2<-numeric(length(DF$Time)) #allocate vector for second derivative estimate at each data point
```

```
tstep<-round(length(DF$Time)/10,0) #determine adequate time step for numerical estimation

#loop through all data points and estimate second derivative.
for (l in tstep:(length(DF$Time)-(tstep-1))){
  curD2<-(DF$DM[l+(tstep-1)]-2*DF$DM[l]+DF$DM[l-(tstep-1)])/((DF$Time[l+tstep/2]-DF$Time[l-tstep/2])^2)
  D2[l]<-curD2
}

#determine time, cycles and stiffness at failure
Tf<-DF$Time[D2==min(D2)]
Nf<-Tf*freq
DMf<-DF$DM[D2==min(D2)]
cycles<-DF$Time*10

#determine initial strain. Arbitrarily set time at which initial is considered, say 200 cycles or 20 s
IS<-DF$Strain[length(DF$Time[DF$Time<200/freq])]
IDM<-DF$DM[length(DF$Time[DF$Time<200/freq])]

#generate stiffness reduction plot
plot(cycles,DF$DM,main = paste("Stiffness Reduction - Specimen ",specnum),xlab = "Cycles",ylab = "Stiffness
[GPa]")
text(cycles[length(cycles)],IDM,paste(Mix,"\nInit. Strain = ",round(IS*10^6,0),"x10^-6\nInit. Stiff. =
",round(IDM,1)," GPa\nAV Content = ",AV,"%"),adj = c(1,0.5))
arrows(Nf,DMf,0,DMf)
arrows(Nf,DMf,Nf,0)
modtext<-(paste("Stiffness @ Fail = ", round(DMf,1)," GPa",sep = ""))
cyctext<-(paste("# Cycles to Fail = ", floor(Nf),sep = ""))
text(Nf-5000,DMf-0.05,paste(modtext,"\n",cyctext,sep = ""),adj = c(1,1))
```

APPENDIX C: SPECIMEN INFORMATION

The table below provides relevant volumetric properties for each of the specimens produced as a part of this study. The blank cells indicate that that property was not measured at the time the specimen was produced or is otherwise unknown.

ID	Mix	Mid-Specimen Width [mm]	Mid-Specimen Thickness [mm]	Area [mm^2]	Arc Radius [mm]	G_{mb}	G_{mm}	Asphalt Content	Air Void Content
KMT001	-	-	-	-	-	-	-	-	-
KMT002	-	83.6	23.8	1990	201	-	-	-	-
KMT003	-	85.7	19.2	1645	202	-	-	-	-
KMT004	-	88.2	25.1	2214	171	-	-	-	-
KMT005	-	90.0	24.5	2205	168	-	-	-	-
KMT006	-	88.3	26.7	2358	176	-	-	-	-
KMT007	-	88.1	21.4	1885	206	-	-	-	-
KMT008	FAA3Q	81.7	25.8	2108	171	-	2.459	5.8%	-
KMT009	FAA3Q	82.9	23.4	1940	172	2.450	2.459	5.8%	0.4%
KMT010	FAA3Q	83.0	24.9	2067	179	2.431	2.459	5.8%	1.1%
KMT011	FAA3Q	93.1	26.3	2451	152	2.419	2.459	5.8%	1.6%
KMT012	STIV	87.9	23.7	2083	156	2.475	2.493	6.2%	0.7%
KMT013	STIV	89.0	23.7	2109	157	2.396	2.493	6.2%	3.9%
KMT014	STIV	86.9	17.8	1547	159	2.460	2.493	6.2%	1.3%
KMT015	STIV-R	86.9	26.3	2285	165	2.463	2.505	6.0%	1.7%
KMT016	STIV-R	84.3	25.9	2183	171	2.364	2.505	6.0%	5.6%
KMT017	STIV-R	84.5	25.9	2189	158	2.449	2.505	6.0%	2.2%
KMT018	STIV	85.2	26.0	2215	165	2.402	2.493	6.2%	3.7%
KMT019	STIV	82.7	26.1	2158	175	2.414	2.493	6.2%	3.2%
KMT020	STIV	85.1	27.1	2306	157	2.341	2.493	6.2%	6.1%
KMT021	STIV-R	84.2	26.0	2190	191	2.369	2.505	6.0%	5.4%
KMT022	STIV-R	86.1	26.8	2310	177	2.338	2.505	6.0%	6.7%
KMT023	STIV-R	83.3	28.0	2330	188	2.387	2.505	6.0%	4.7%
KMT024	FAA3Q	86.4	26.8	2312	195	2.414	2.459	5.8%	1.8%
KMT025	FAA3Q	85.3	27.3	2329	193	2.466	2.459	5.8%	-0.3%
KMT026	FAA3Q	86.1	27.8	2396	184	2.402	2.459	5.8%	2.3%
KMT027	FAA3Q	86.3	28.1	2429	178	2.405	2.459	5.8%	2.2%
KMT028	FAA3Q	85.8	27.7	2375	191	2.453	2.459	5.8%	0.3%
KMT029	FAA3Q	88.6	27.9	2472	181	2.419	2.459	5.8%	1.6%
KMT032	TLO	96.1	40.0	3847	166	2.403	2.439	7.5%	1.5%

ID	Mix	Mid-Specimen Width [mm]	Mid-Specimen Thickness [mm]	Area [mm^2]	Arc Radius [mm]	G_{mb}	G_{mm}	Asphalt Content	Air Void Content
KMT033	TLO	93.9	39.1	3671	177	2.388	2.439	7.5%	2.1%
KMT034	TLO	99.4	36.2	3598	182	2.423	2.439	7.5%	0.6%
KMT035	TLO	100.3	87.9	8816	185	2.438	2.439	7.5%	0.0%
KMT036	TLO	81.9	40.3	3301	191	2.404	2.439	7.5%	1.4%
KMT037	TLO	80.9	31.5	2549	195	2.410	2.439	7.5%	1.2%
KMT038	TLO	85.4	38.5	3289	201	2.405	2.439	7.5%	1.4%
KMT039	TLO	82.8	40.1	3323	194	2.383	2.439	7.5%	2.3%

APPENDIX D: STIFFNESS REDUCTION PLOTS

This appendix provides the stiffness reduction plots for all tests successfully resulting in a mid-specimen failure. The first several tests were conceptual in nature and insufficient data was acquired during these tests. As a result, stiffness reduction plots for these tests are not included. In the plots, the stiffness of the specimen is plotted against the number of cycles. The number of cycles to failure and stiffness at failure is indicated. Additionally, the mixture, asphalt content, initial strain, initial stiffness and air void content for the specimen is provided. The initial strain and stiffness are taken at cycle number 200. For more information regarding the criteria for failure and determination of strain amplitude and stiffness, refer to CHAPTER 5: TEST RESULTS AND ANALYSIS.

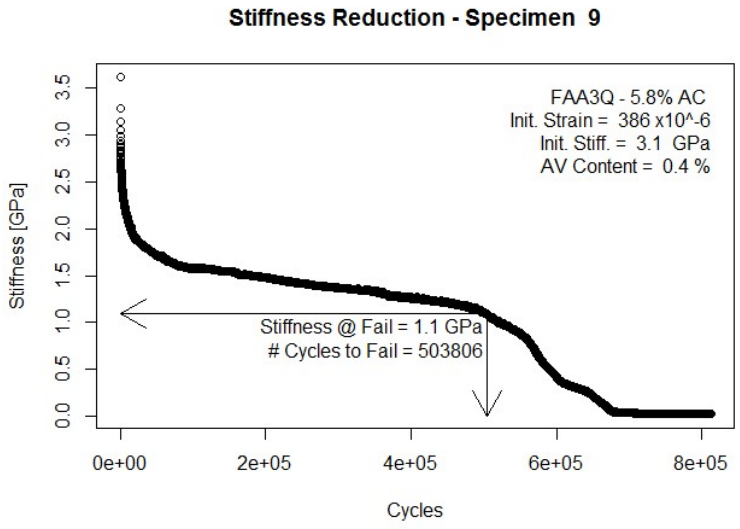

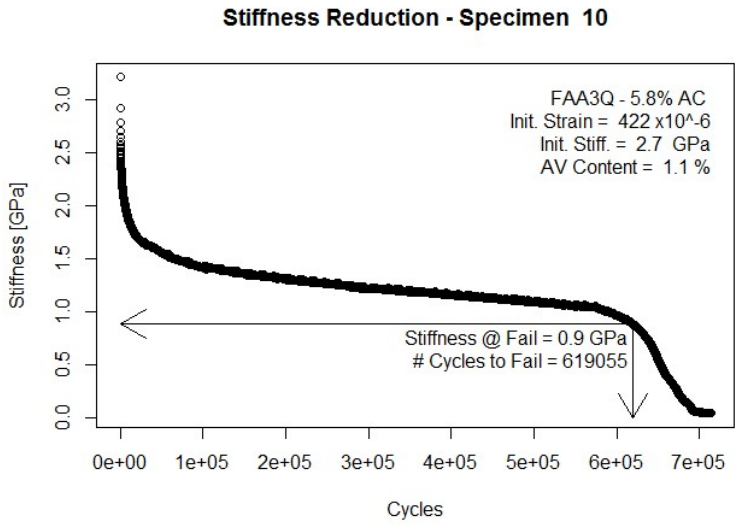
Stiffness Reduction - Specimen 10
FAA3Q - 5.8% AC
Init. Strain = 422 x10^-6
Init. Stiff. = 2.7 GPa
AV Content = 1.1 %
Stiffness @ Fail = 0.9 GPa
Cycles to Fail = 619055
Stiffness [GPa]
0.0
0.5
1.0
1.5
2.0
2.5
3.0
0e+00
1e+05
2e+05
3e+05
4e+05
5e+05
6e+05
7e+05
Cycles

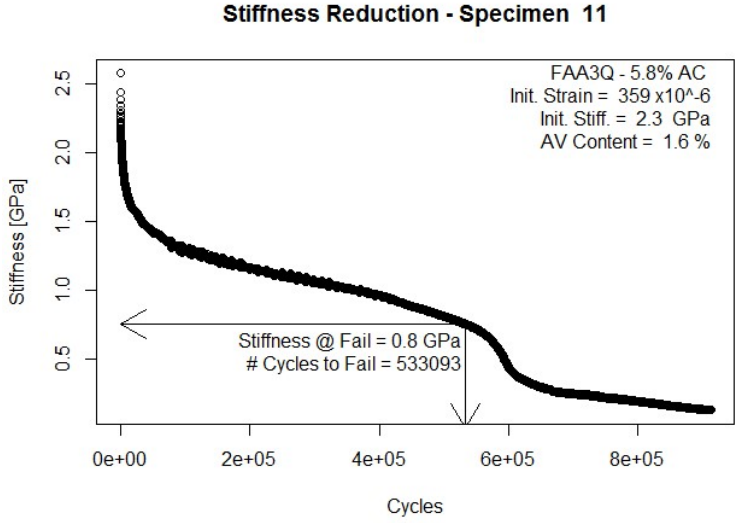
Stiffness Reduction - Specimen 11
FAA3Q - 5.8% AC
Init. Strain = 359 x10^-6
Init. Stiff. = 2.3 GPa
AV Content = 1.6 %
Stiffness @ Fail = 0.8 GPa
Cycles to Fail = 533093
Stiffness [GPa]
0.5
1.0
1.5
2.0
2.5
0e+00
2e+05
4e+05
6e+05
8e+05
Cycles

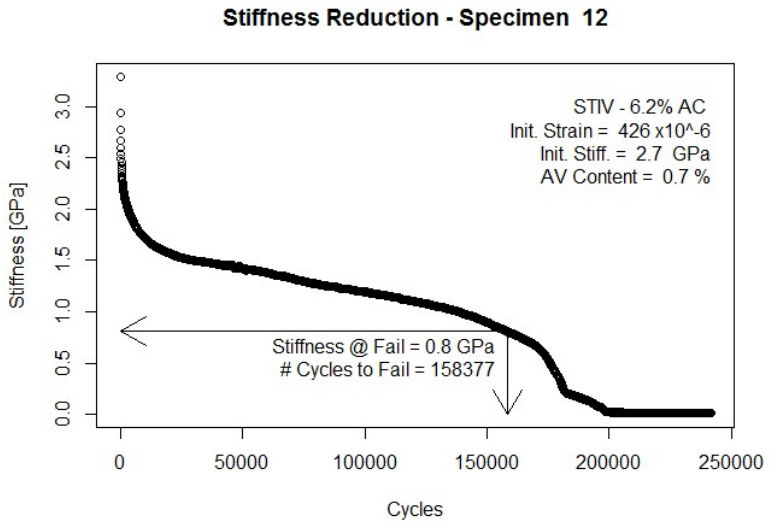
Stiffness Reduction - Specimen 12
STIV - 6.2% AC
Init. Strain = 426 x10^-6
Init. Stiff. = 2.7 GPa
AV Content = 0.7 %
Stiffness @ Fail = 0.8 GPa
Cycles to Fail = 158377
Stiffness [GPa]
0.0
0.5
1.0
1.5
2.0
2.5
3.0
0
50000
100000
150000
200000
250000
Cycles

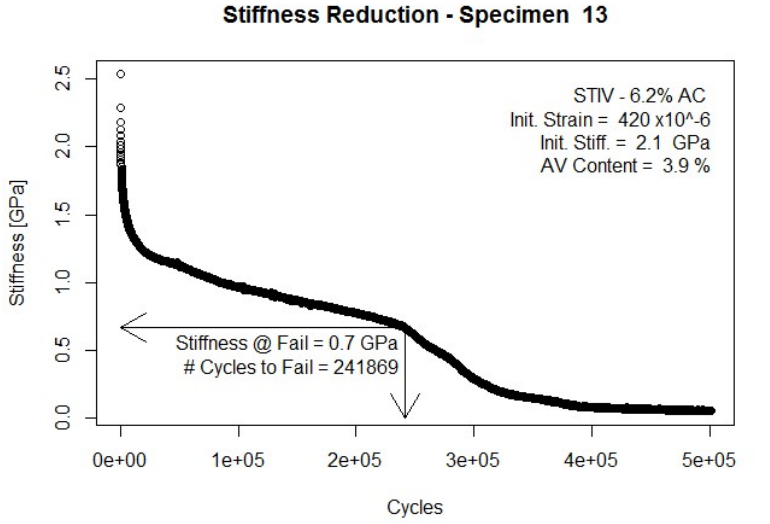
Stiffness Reduction - Specimen 13
STIV - 6.2% AC
Init. Strain = 420 x10^-6
Init. Stiff. = 2.1 GPa
AV Content = 3.9 %
Stiffness @ Fail = 0.7 GPa
Cycles to Fail = 241869
Stiffness [GPa]
0.0
0.5
1.0
1.5
2.0
2.5
0e+00
1e+05
2e+05
3e+05
4e+05
5e+05
Cycles

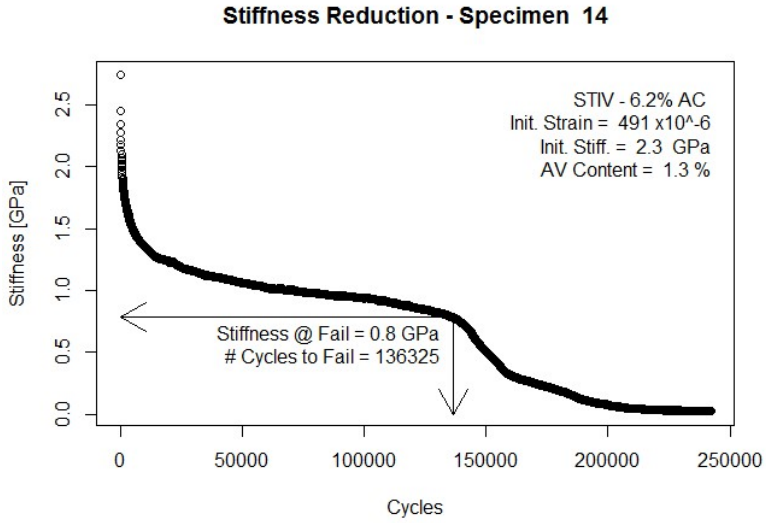
Stiffness Reduction - Specimen 14
STIV - 6.2% AC
Init. Strain = 491 x10^-6
Init. Stiff. = 2.3 GPa
AV Content = 1.3 %
Stiffness @ Fail = 0.8 GPa
Cycles to Fail = 136325
Stiffness [GPa]
0.0
0.5
1.0
1.5
2.0
2.5
0
50000
100000
150000
200000
250000
Cycles

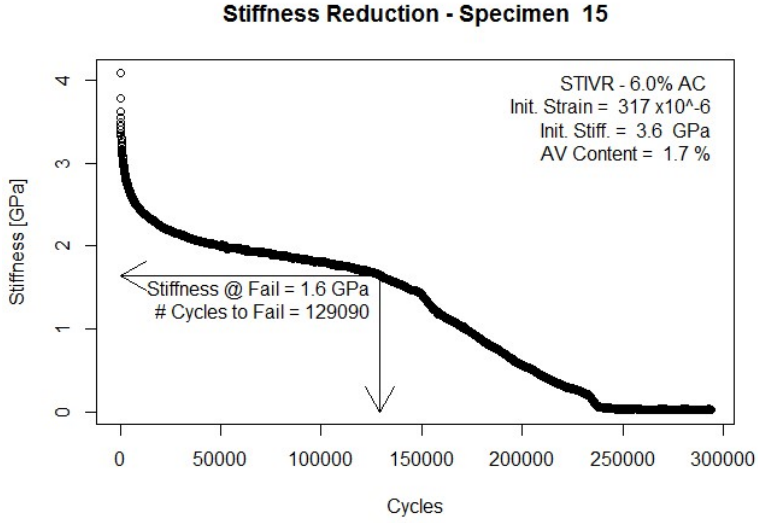
Stiffness Reduction - Specimen 15
STIVR - 6.0% AC
Init. Strain = 317 x10^-6
Init. Stiff. = 3.6 GPa
AV Content = 1.7 %
Stiffness @ Fail = 1.6 GPa
Cycles to Fail = 129090
Stiffness [GPa]
0
1
2
3
4
0
50000
100000
150000
200000
250000
300000
Cycles

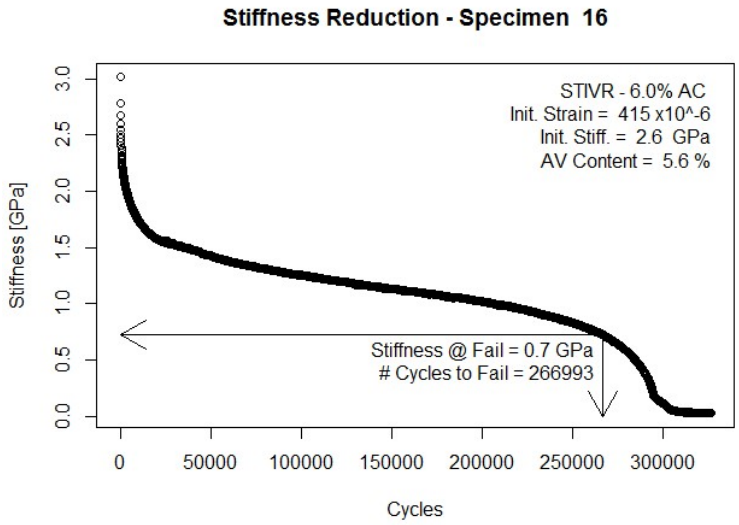
Stiffness Reduction - Specimen 16
STIVR - 6.0% AC
Init. Strain = 415 x10^-6
Init. Stiff. = 2.6 GPa
AV Content = 5.6 %
Stiffness @ Fail = 0.7 GPa
Cycles to Fail = 266993
Stiffness [GPa]
0.0
0.5
1.0
1.5
2.0
2.5
3.0
0
50000
100000
150000
200000
250000
300000
Cycles

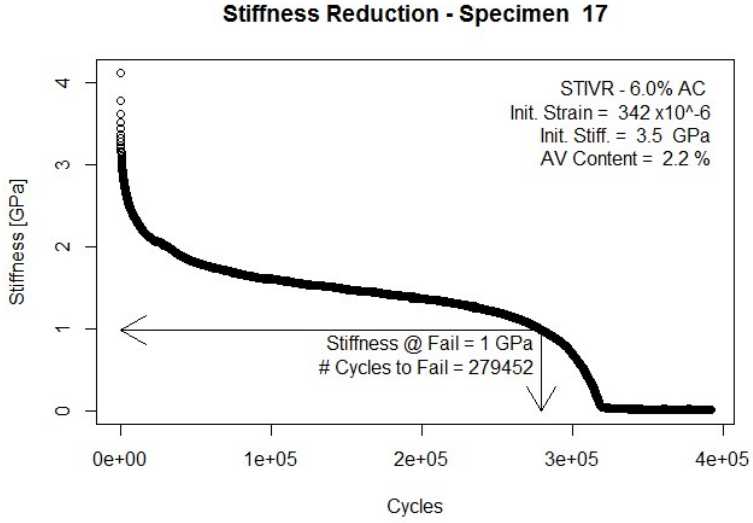
Stiffness Reduction - Specimen 17
STIVR - 6.0% AC
Init. Strain = 342 x10^-6
Init. Stiff. = 3.5 GPa
AV Content = 2.2 %
Stiffness @ Fail = 1 GPa
Cycles to Fail = 279452
Stiffness [GPa]
0
1
2
3
4
0e+00
1e+05
2e+05
3e+05
4e+05
Cycles

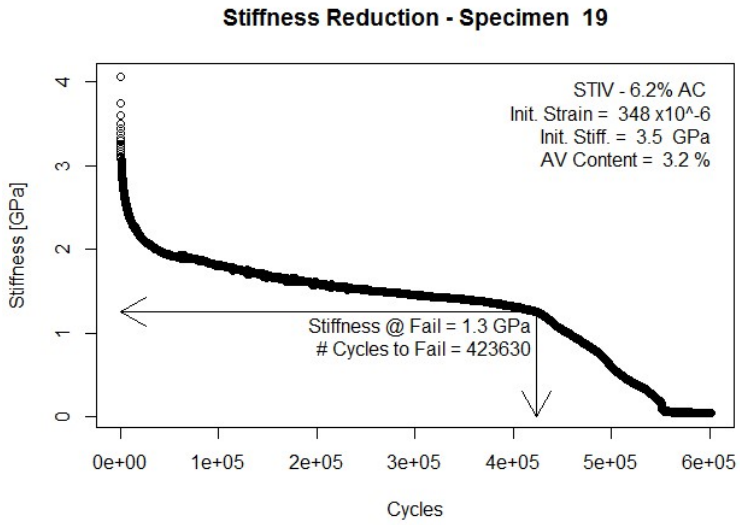
Stiffness Reduction - Specimen 19
STIV - 6.2% AC
Init. Strain = 348 x10^-6
Init. Stiff. = 3.5 GPa
AV Content = 3.2 %
Stiffness @ Fail = 1.3 GPa
Cycles to Fail = 423630
Stiffness [GPa]
Cycles
0e+00
1e+05
2e+05
3e+05
4e+05
5e+05
6e+05
0
1
2
3
4

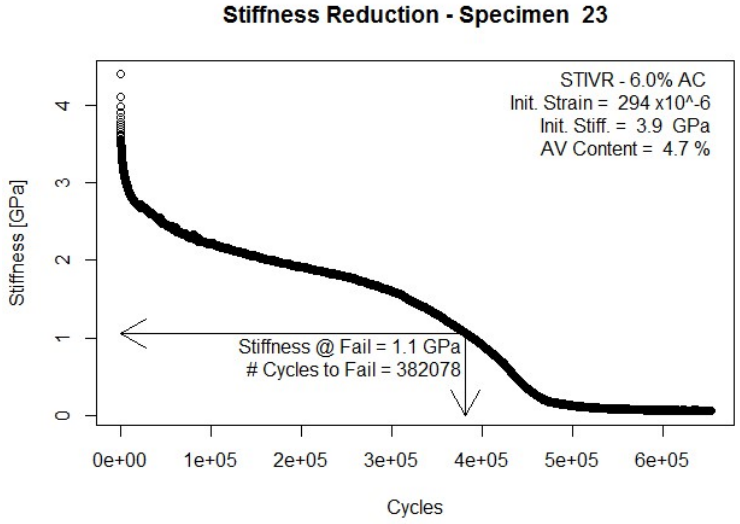
Stiffness Reduction - Specimen 23
STIVR - 6.0% AC
Init. Strain = 294 x10^-6
Init. Stiff. = 3.9 GPa
AV Content = 4.7 %
Stiffness @ Fail = 1.1 GPa
Cycles to Fail = 382078
Stiffness [GPa]
Cycles
0e+00
1e+05
2e+05
3e+05
4e+05
5e+05
6e+05
0
1
2
3
4

3

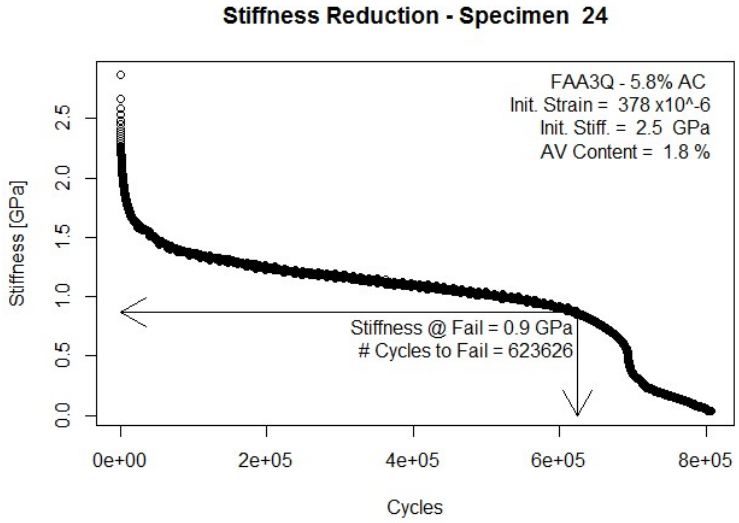
Stiffness Reduction - Specimen 24
FAA3Q - 5.8% AC
Init. Strain = 378 x10^-6
Init. Stiff. = 2.5 GPa
AV Content = 1.8 %
Stiffness @ Fail = 0.9 GPa
Cycles to Fail = 623626
Stiffness [GPa]
0.0
0.5
1.0
1.5
2.0
2.5
0e+00
2e+05
4e+05
6e+05
8e+05
Cycles

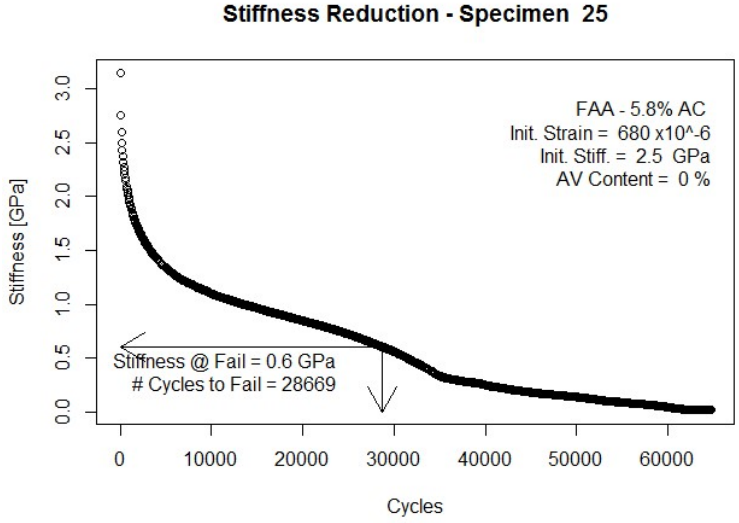
Stiffness Reduction - Specimen 25
FAA - 5.8% AC
Init. Strain = 680 x10^-6
Init. Stiff. = 2.5 GPa
AV Content = 0 %
Stiffness @ Fail = 0.6 GPa
Cycles to Fail = 28669
Stiffness [GPa]
0.0
0.5
1.0
1.5
2.0
2.5
3.0
0
10000
20000
30000
40000
50000
60000
Cycles

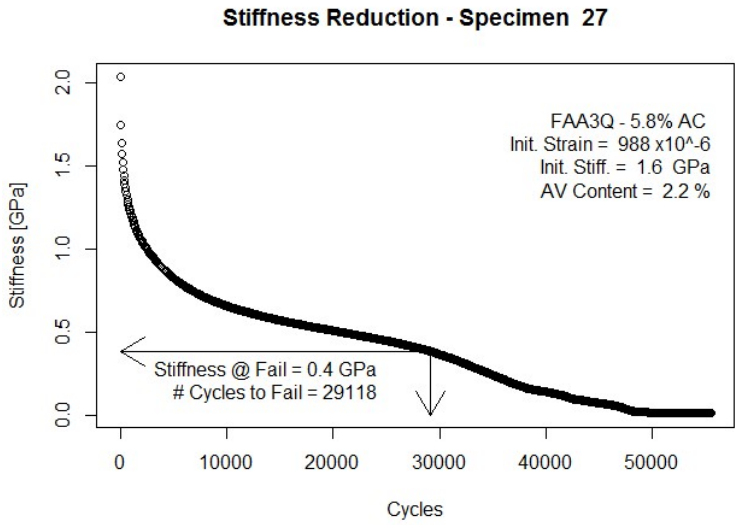
Stiffness Reduction - Specimen 27
FAA3Q - 5.8% AC
Init. Strain = 988 x10^-6
Init. Stiff. = 1.6 GPa
AV Content = 2.2 %
Stiffness @ Fail = 0.4 GPa
Cycles to Fail = 29118
Stiffness [GPa]
0.0
0.5
1.0
1.5
2.0
0
10000
20000
30000
40000
50000
Cycles

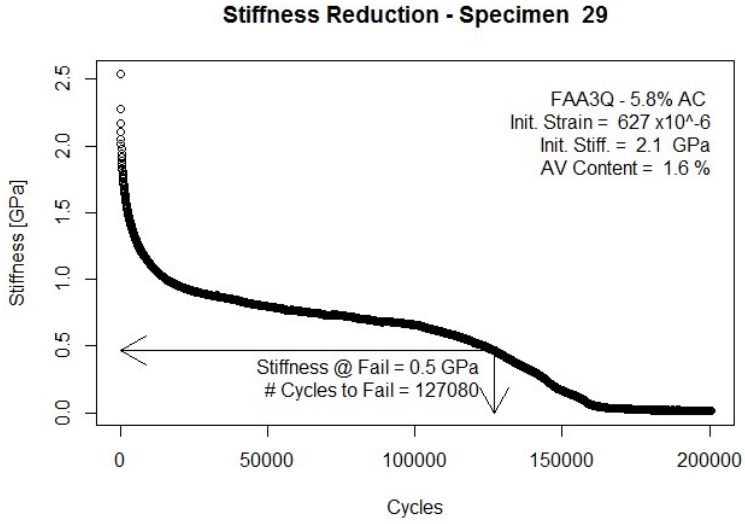
Stiffness Reduction - Specimen 29
FAA3Q - 5.8% AC
Init. Strain = 627 x10^-6
Init. Stiff. = 2.1 GPa
AV Content = 1.6 %
Stiffness @ Fail = 0.5 GPa
Cycles to Fail = 127080
Stiffness [GPa]
0.0
0.5
1.0
1.5
2.0
2.5
0
50000
100000
150000
200000
Cycles

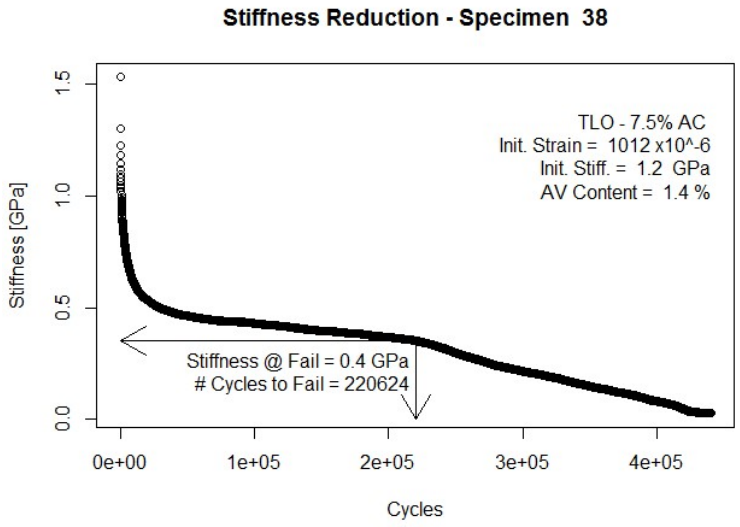
Stiffness Reduction - Specimen 38
TLO - 7.5% AC
Init. Strain = 1012 x10^-6
Init. Stiff. = 1.2 GPa
AV Content = 1.4 %
Stiffness @ Fail = 0.4 GPa
Cycles to Fail = 220624
Stiffness [GPa]
0.0
0.5
1.0
1.5
0e+00
1e+05
2e+05
3e+05
4e+05
Cycles

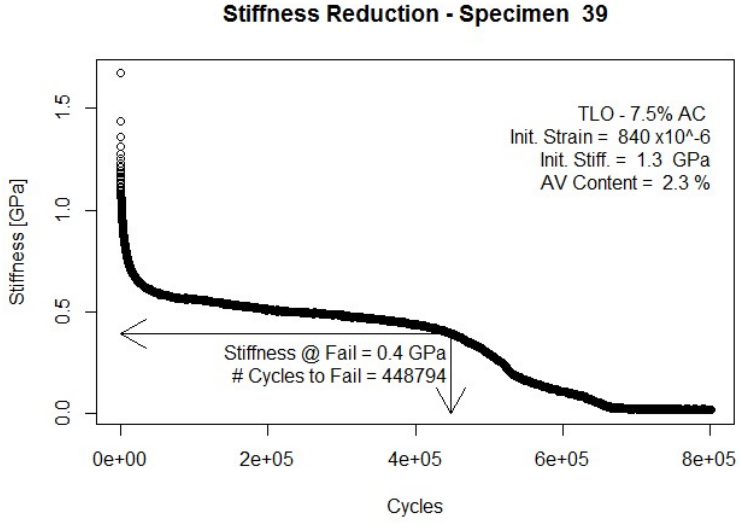
Stiffness Reduction - Specimen 39
TLO - 7.5% AC
Init. Strain = 840 x10^-6
Init. Stiff. = 1.3 GPa
AV Content = 2.3 %
Stiffness @ Fail = 0.4 GPa
Cycles to Fail = 448794
Stiffness [GPa]
0.0
0.5
1.0
1.5
0e+00
2e+05
4e+05
6e+05
8e+05
Cycles

REFERENCES

AASHTO. (2016). Standard Specifications for Transportation Materials and Methods of Sampling and Testing and AASHTO Provisional Standards. Washington D.C.: American Association of State Highway and Transportation Officials.

Anagnos, J. N., & Kennedy, T. W. (1983). *Procedures for the Static and Repeated-Load Indirect Tensile Tests*. Research Record 183-14, Center for Transportation Research, University of Texas at Austin.

Archilla, A. R. (2015). Top-Down Fatigue Cracking in High-Temperature Environments. *Transportation Research Record: Journal of the Transportation Research Board, 2507*, Transportation Research Board of the National Academies, Washington, D.C.128-137.

Archilla, A. R., & Corrales-Azofeifa, J. (2017). *Development of Asphalt Concrete Dogbone Shape Specimens for Uniaxial Tension Testing*. Paper presented at the Airfield and Highway Pavements 2017.

ASTM. (2016). E8/E8M-16a, Standard Test Methods for Tension Testing of Metallic Materials. West Conshohocken, PA: ASTM International.

ASTM. (2017). ASTM D6931-17 Standard Test Method for Indirect Tensile (IDT) Strength of Asphalt Mixtures. West Conshohocken, PA: ASTM International.

Bonaquist, R. F. (2008). *Refining the Simple Performance Tester for use in Routine Practice*. Washington, D.C.: Transportation Research Board.

Castorena, C., Kim, Y. R., Pape, S., & Lee, K. (2017). Development of Small Specimen Geometry for Asphalt Mixture Performance Testing. *NCHRP IDEA Program* (Vol. 181). Washington D.C.: Transportation Research Board.

Chehab, G., O'Quinn, E., & Kim, Y. R. (2000). Specimen Geometry Study for Direct Tension Test Based on Mechanical Tests and Air Void Variation in Asphalt Concrete Specimens Compacted by Superpave Gyratory Compactor. *Transportation Research Record: Journal of the Transportation Research Board*(1723), Transportation Research Board of the National Academies, Washington, D.C. 125-132.

Cowher, C. E., & Kennedy, T. W. (1975). Report 183-3: Cumulative Damage of Asphalt Materials under Repeated-Load Indirect Tension. Center for Transportation Research, University of Texas at Austin.

Deacon, J. A. (1965). *Fatigue of Asphalt Concrete.* (Doctor of Engineering), University of California Berkeley.

Epps, J. A., & Monismith, C. L. (1972). Fatigue of Asphalt Concrete Mixtures—Summary of Existing Information. *Fatigue of compacted bituminous aggregate mixtures*: ASTM International.

Erkens, S., & Poot, M. (2001). The Uniaxial Tension Test–Asphalt Concrete Response (ACRe). *Delft University of Technology Report*(7-01), 117-117.

Ghuzlan, K. A., & Carpenter, S. H. (2006). Fatigue Damage Analysis in Asphalt Concrete Mixtures Using the Dissipated Energy Approach. Canadian Journal of Civil Engineering, 33(7), 890-901.

Hou, T. (2009). *Fatigue Performance Prediction of North Carolina Mixtures using Simplified Viscoelastic Continuum Damage Model.* (Master of Science), North Carolina State University.

Hveem, F., & Carmany, R. (1949). *The Factors Underlying the Rational Design of Pavements.* Paper presented at the Highway Research Board Proceedings.

Kallas, B. (1970). *Dynamic Modulus of Asphalt Concrete in Tension and Tension-Compression and Discussion.* Paper presented at the Association of Asphalt Paving Technologists Proc.

Kim, Y. R., & Little, D. N. (1990). One-Dimensional Constitutive Modeling of Asphalt Concrete. *Journal of Engineering Mechanics, 116*(4), 751-772.

Kutay, M., Gibson, N., Youtcheff, J., & Dongré, R. (2009). Use of Small Samples to Predict Fatigue Lives of Field Cores: Newly Developed Formulation Based on Viscoelastic Continuum Damage Theory. *Transportation Research Record: Journal of the Transportation Research Board, 2127*, Transportation Research Board of the National Academies, Washington, D.C. 90-97.

Lee, J.-S., Norouzi, A., & Kim, Y. R. (2016). Determining Specimen Geometry of Cylindrical Specimens for Direct Tension Fatigue Testing of Asphalt Concrete. *ASTM Journal of Testing and Evaluation, 45*(2), 613-623.

Park, S. W., Kim, Y. R., & Schapery, R. A. (1996). A Viscoelastic Continuum Damage Model and its Application to Uniaxial Behavior of Asphalt Concrete. *Mechanics of Materials, 24*(4), 241-255.

Pell, P. S., McCarthy, P. F., & Gardner, R. R. (1961). Fatigue of Bitumen and Bituminous Mixes. *International Journal of Mechanical Sciences, 3*(4).

Porter, B. W., & Kennedy, T. W. (1975). Report 183-4: Comparison of Fatigue Test Methods for Asphalt Materials. Research Record 183-4, Center for Transportation Research, University of Texas at Austin.

Raithby, K., & Sterling, A. (1972). TRRL Report LR 496: Some Effects of Loading History on the Fatigue Performance of Rolled Asphalt. Crowthorne, Berkshire, United Kingdom: Transport and Road Research Laboratory.

Reese, R. (1997). Properties of Aged Asphalt Binder Related to Asphalt Concrete Fatigue Life. *Journal of the Association of Asphalt Paving Technologists, 66*.

Sabouri, M. (2014). *Development of a Unified Fatigue Failure Criterion for Asphalt Mixtures and its Applications to Reclaimed Asphalt Pavement (RAP) Mixtures.* (Doctor of Philosophy), North Carolina State University.

Schapery, R. (1984). Correspondence Principles and a Generalized J Integral for Large Deformation and Fracture Analysis of Viscoelastic Media. *International Journal of Fracture, 25*(3), 195-223.

Superpave Mix Design, Superpave Series No. 2 (SP-2). (1996). Lexington, KY: The Asphalt Institute.

Tangella, S. R., Craus, J., Deacon, J., & Monismith, C. (1990). Summary Report on Fatigue Response of Asphalt Mixtures. In *SHRP Project A-003-A*. Berkeley, California: Institute of Transportation Studies, University of California.

Witzcak, M. W. (2002). NCHRP Report 465: Simple Performance Test for Superpave Mix Design. Washington, D.C.: National Academy Press.

Zhou, F., Hu, S., Chen, D.-H., & Scullion, T. (2007). Overlay Tester: Simple Performance Test for Fatigue Cracking. *Transportation Research Record: Journal of the Transportation Research Board*(2001), 1-8.